AN ABSTRACT OF THE THESIS OF

Sunil Kapoor for the degree of Master of Science in Electrical and Computer Engineering presented on July 31, 1992.

Title : Analysis of Interacting Discontinuities in Microstrips by Mode Matching Technique

Abstract approved: _____ Vijai K. Tripathi

In this thesis a numerical technique to model general microstrip asymmetric and multiple step discontinuities is presented. The method is based on a magnetic wall waveguide model that is assumed to be valid for describing the electromagnetic fields associated with the microstrip line and in the vicinity of microstrip discontinuities. The fields are expanded in the uniform regions and the mode-matching method is applied at the discontinuities to analyze for the frequency dependent transmission properties of the multi ports. The generalized scattering matrix technique is used to model cascaded interacting discontinuities and is used to compute the properties of double-step and multi port structures. The generalized scattering matrix formulation takes into account the scattering phenomena of the dominant and all of the higher-order modes including evanescent ones.

The validity of this model has been discussed extensively, and it is shown that the model can be used to describe the microstrip discontinuities with acceptable accuracy. The technique is applied (1) to study the transmission characteristics of asymmetric step discontinuities; (2) to design a filter for a desired frequency range using interacting asymmetric double step microstrip line; and (3) to design a new nominal 3db power devider of large bandwidth consisting of a three port rectangular patch. The techniques and models presented can be used in computer-aided analysis and design of such circuits.

ANALYSIS OF INTERACTING DISCONTINUITIES IN MICROSTRIPS BY MODE-MATCHING TECHNIQUE

by

Sunil Kapoor

A THESIS

submitted to

Oregon State University

in partial fulfillment of
the requirements for the
degree of

Master of Science

Completed July 31, 1992

Commencement June 1993

APPROVED :

Redacted for Privacy

Professor of Electrical and Computer Engineering in charge of major

Redacted for Privacy

Head of department of Electrical and Computer Engineering

Redacted for Privacy

Dean of Graduate School

Date thesis is presented July 31, 1992

Typed by Sunil Kapoor

ACKNOWLEDGEMENTS

A number of persons have contributed to the progress of this thesis. Of these thanks are due to my colleague Andreas Weisshaar who helped me in removing bugs from the software. Further thanks go to my roommates Sanjeev Qazi and Arbinda Bose who have been a constant source of encouragement and understanding during the many frustrating stages of my M.S. program. I am also grateful to Ms Uma Krishnan who helped me in making figures and gave some valuable suggestions for this report.

I sincerely appreciate the advice and encouragement given by my major professor Vijai K. Tripathi. The guidance I received from Prof. Tripathi as my thesis advisor is gratefully acknowledged. Prof. Tripathi also provided financial support during the crucial period of this thesis. I am also grateful to the members of my graduate committee for their time and advice.

I sincerely thank my parents, M. Raj and Usha Kapoor, for their understanding and encouragement of my studies abroad.

TABLE OF CONTENTS

LIST OF FIGURES

CHAPTER 1

ANALYSIS OF INTERACTING DISCONTINUITIES IN MICROSTRIPS BY MODE MATCHING TECHNIQUE

INTRODUCTION

Many modern high frequency integrated circuits, in the microwave and millimeter-wave frequency range, are hybrid or monolithic integrated circuits based on planar transmission line techniques. The transmission line used in most of these circuits is the microstrip line or asymmetrical stripline. A microstrip line consists of a dielectric substrate material of height h and relative dielectric constant ϵ_r having a metallic strip of width w and metallization thickness t forming the wave guiding structure. The planar, distributed and passive components used in these microwave integrated circuits consist of planar transmission lines and microstrip discontinuities. Advances in microwave and millimeter-wave integrated circuits, particularly in the monolithic form, have increased the necessity of accurate computer-aided design (CAD). Unlike hybrid microwave integrated circuits at low frequencies, it is extremely difficult to adjust the characteristics of monolithic circuits once they are fabricated. Therefore an accurate CAD program is essential for design of these circuits. It is therefore an essential task to accurately model the frequency-dependent transmission properties of these subcomponents(discontinuities), if accurate CAD techniques for the analysis and synthesis of microwave integrated circuits are to be established. The microstrip line and its frequency-dependent properties in the meantime can be described by simple empirical formulas that accurately model the results of efficient numerical

methods for the calculation of the phase velocities and the characteristic impedances of the fundamental and the higher-order modes [1,2]. For the analysis of the microstrip discontinuities, such as bends, steps and junctions, three types of basic models have been reported.

1. Equivalent circuits consisting of lumped elements (capacitances, inductances and resistances) are used to describe the discontinuities and are calculated using quasi-static or stationary methods. The advantage of this method is that it leads to simple formulas describing the equivalent circuit elements, but the disadvantage being that these formulas have only a restricted validity range (frequency, substrate materials, line widths) for their application.
2. The wave properties of the electromagnetic fields on the microstrip structures are taken into account to describe more accurately the frequency-dependent properties of the discontinuities. A first approximate way in which this can be done is to apply a waveguide model of the microstrip line for modelling the electromagnetic fields near microstrip discontinuities. This method is a compromise between the requirement for more accurate and more broadband models for microstrip discontinuities and the requirement for the small numerical effort so that the models can be used directly in the desktop computer programs.
3. Constructing complete electromagnetic field solution for associated boundary value problem, an exact analysis of discontinuities can be conducted.

The objective of this report is to formulate a computer aided design procedure for characterizing a class of asymmetric microstrip discontinuities by using the equivalent waveguiding model. As is well known, the microstrip line is an open waveguide structure, and the associated electromagnetic fields are unbounded. A metallic shielding or a metallic cover plate of infinite dimensions above the line is used to define well-determined boundary conditions for the field to analyse it numerically. Because of the inhomogeneous dielectric field region (substrate material/air space) the electromagnetic fields on the microstrip line are represented by hybrid modes; that is, the electric field strength and magnetic field strength always have three field components. These hybrid modes can be classified as EH or HE modes. The field distributions of the electric and magnetic field strengths of the fundamental EH mode (quasi-TEM mode) on a covered microstrip line has been computed by Ermert[3] on the basis of rigorous field analysis.

Due to the hybrid field nature of the microstrip line, the parameters describing wave propagation, even in the case of the fundamental mode, are frequency dependent. Several approaches have been published to describe these line parameters by static methods [4,5], by models of a different kind to simulate the frequency dependence of the parameters, or by rigorous numerical field analysis methods. A rigorous solution using numerical field analysis always requires a relatively high degree of numerical efforts. As a result the analysis of microstrip discontinuities using these numerical solutions of the electromagnetic fields always leads to long computation

times and normally cannot be used for direct application in computer-aided circuit design techniques. A rigorous solution can help facilitate the development of simple approximate formulas or models for the discontinuities.

Wheeler [4,5] proposed a waveguide model for the microstrip line to fulfill the requirements that

1. The waveguide model must describe the electromagnetic fields and the characteristic line parameters (characteristic impedance and phase velocity) of the fundamental quasi-TEM mode on the microstrip line with high accuracy over the frequency range at least up to the cutoff frequency of the first higher-order mode.
2. The cut-off frequencies and the electromagnetic fields of the higher-order modes must be modelled so that the application of these higher-order modes to the analysis of the microstrip discontinuities leads to acceptable accuracy.
3. The model must be simple enough so that well-known numerical methods for analyzing ideal waveguide discontinuities that include the energy stored near the discontinuities can be used, thereby taking into account the frequency-dependent transmission properties of these structures.

Figure 1 shows how Wheeler[4,5] analyzed the microstrip line. A conformal mapping technique can be used to transform the electric field in a cross section of the microstrip line into the field of an ideal parallel-plate waveguide as shown in figure 1, assuming that the fundamental EH mode on the microstrip line is a quasi-TEM mode (which is correct at least at low frequencies). The conformal mapping

techniques give essential relations in simple forms in terms of "slide rule" functions. This ideal waveguide has no stray fields as it is closed by magnetic side walls and has electric walls on its top and bottom. Height h of the waveguide is assumed to be identical to height of the substrate material. Width w_{eff} of this waveguide can be found from conformal mapping technique and is given in the publications of Wheeler for static case. The conformal mapping technique is intended to serve a variety of purposes, as follows[4]:

1) To enable the reliable computation of this case, in terms of "slide rule" functions, close enough for the most exacting requirements of mathematical scrutiny.
2) To yield simple approximate formulas for practical computations to "slide rule" accuracy, and for showing clearly the principal effects of the variables.
3) To present a method of simple approximation in conformal mapping, applicable to various configurations of wide strip conductors, and susceptible of determination within close limits of error. The method is a departure from the straightforward exact procedure.

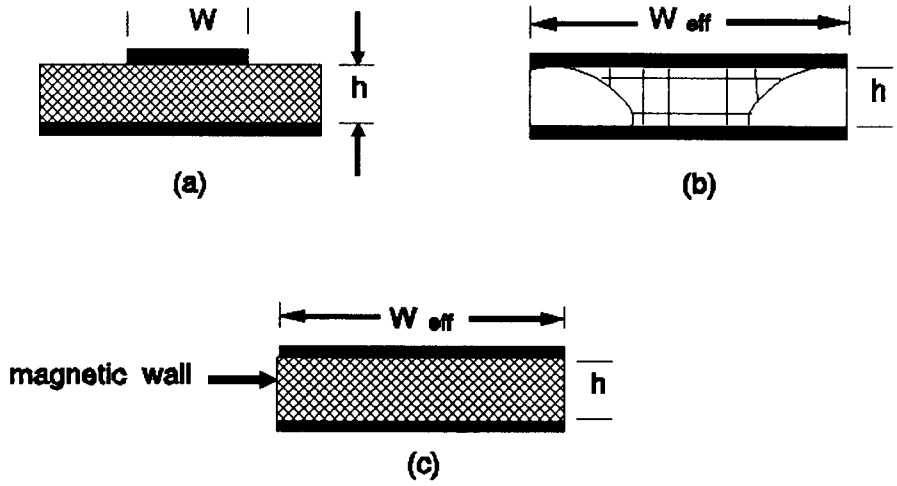

Figure 1 The microstrip line (a) and its waveguide model (c), which has been developed using a conformal mapping technique. Figure (b) shows in principle how the dielectric-air interface is transformed by conformal mapping technique.

If the microstrip line is transformed into the waveguide model, the waveguide is only partly filled by dielectric material of relative dielectric constant ϵ_r, and an air-dielectric interface is formed. To simplify the waveguide model, it is filled with a homogeneous dielectric medium instead of the inhomogeneous medium so that the phase velocity of the fundamental wave in the final waveguide model is identical to the phase velocity of the fundamental wave on the microstrip line.

At low frequencies the longitudinal components of the electromagnetic fields of the microstrip line are small and the field is nearly a TEM mode and the conformal mapping technique can be applied. Thus the waveguide model describes correctly the transmission properties of the fundamental quasi-TEM mode for very low frequencies. The effective dielectric constant ϵ_{eff} and the effective width w_{eff} can be calculated using Wheeler's formulas:

$$\epsilon_{eff} = \left(\sqrt{\epsilon_r} + \frac{(\epsilon_r - 1)\left[\ln(\pi/4)^2 + 1 - \epsilon_r \ln(\pi e/2)\,(w/2h + 0.94)\right]}{2\sqrt{\epsilon_r}\,\epsilon_r\,(w\pi/2h + \ln[2\pi e\,(w/2h + 0.94)])}\right)^2 \qquad (1)$$

$$w_{eff} = (w/h + (2/\pi)\ln[2\pi e((w/2h) + 0.92)])\,h \qquad (2)$$

The phase velocity v_{ph} of the fundamental quasi-TEM mode and its characteristic impedance for low frequencies can be calculated as the parameters of the fundamental mode of the waveguide model using (1) and (2).

$$v_{ph} = \frac{c_0}{\sqrt{\epsilon_{eff}}} \qquad (3)$$

and

$$Z_0 = \sqrt{\frac{\mu_0}{\epsilon_0}} \frac{h}{\sqrt{\epsilon_{eff}} w_{eff}} \qquad (4)$$

where c_0 is the velocity of light. The parameters calculated in this way are in agreement with the normal definitions for the microstrip line.

The phase velocity and the characteristic impedance of the fundamental mode (and all the higher-order modes) are frequency dependent due to the hybrid nature of the microstrip fields which leads to dispersive behavior of the line parameters. This means that with increasing frequency the electromagnetic field is more and more concentrated under the strip of the microstripline until at very high frequencies the stray field in the air region vanishes and the field is only in the dielectric substrate material. As a result, the effective dielectric constant ϵ_{eff} converges into the relative dielectric constant ϵ_r and the effective width w_{eff} into the line width w for increasing frequencies. As a consequence of this physical phenomenon, the phase velocity and therefore the effective dielectric constant become frequency-dependent. At very low frequencies the fundamental mode on the microstrip line is a quasi-TEM mode with electromagnetic fields in the air and in the dielectric substrate material. With increasing frequency, the influence of the air-dielectric interface changes the field of the fundamental mode into an EH mode with six field components until very high frequencies, where the field is concentrated in the dielectric material and the field distribution now is nearly a TEM mode again.

The effective dielectric constant and its frequency dependence are a measure of the dispersion of the phase velocity of the waves on the microstrip lines. As explained above, the effective dielectric constant of the waveguide model has been chosen in such a way that the phase velocity of a wave on the line is identical with that of the waves on the original microstrip line. This means that the effective dielectric constant of the original microstrip line and its waveguide model must be identical, and therefore at higher frequencies the effective dielectric constant of the waveguide model must be replaced by the frequency-dependent effective dielectric constant as described above. If the waveguide model is to simulate the wave transmission on the microstrip line correctly, it must also be made sure that the characteristic impedances of the two structures are identical. The characteristic impedance of the waveguide model corresponds to the impedance of the ideal parallel plate structure with electric and magnetic walls and is given by

$$Z_0(f) = \sqrt{\frac{\mu_0}{\epsilon_0}} \frac{h}{\sqrt{\epsilon_{eff}(f)}\, w_{eff}(f)} \qquad (5)$$

Thus the effective line width w_{eff} can be written as,

$$w_{eff}(f) = \sqrt{\frac{\mu_0}{\epsilon_0}} \frac{h}{\sqrt{\epsilon_{eff}(f)}\, Z_0(f)} \qquad (6)$$

and if the effective dielectric constant and the characteristic impedance are replaced by the equivalent frequency-dependent values, a frequency-dependent effective line width $w_{eff}(f)$ is derived that, if applied to the waveguide model, makes sure that the characteristic impedance of the microstrip line is also modeled correctly at each

frequency. The waveguide model can be used to model the transmission properties of the fundamental mode on the microstrip accurately with the defined properties, if the design formulas used for $Z_o(f)$ and $\epsilon_{eff}(f)$ are accurate enough.

The solution for the electromagnetic fields of the waveguide model can be found in the same way as for metallic waveguides. The boundary conditions on the electric walls and the magnetic walls are

$$E \times \overline{n_1} = 0, \qquad H \times \overline{n_2} = 0 \tag{7}$$

where n_1 and n_2 are unit surface vectors on the electric walls and on the magnetic walls, respectively. The field solutions are of TEM, TE(H), and TM(E) modes; their electromagnetic fields can be described by forward and backward traveling waves. In the case of a forward traveling wave, the fields are given by

$$\overline{E_t} = A\overline{g_t}(x,y)\, e^{-\gamma z} \tag{8a}$$

$$\overline{H_t} = \frac{A}{Z_F}\left[\overline{u_z} \times \overline{g_t}(x,y)\right] e^{-\gamma z} \tag{8b}$$

$$E_z = \frac{A}{\gamma}\nabla_t \cdot \overline{g_t}(x,y)\, e^{-\gamma z} \tag{8c}$$

$$H_z = \frac{A}{\gamma Z_F}\nabla_t \cdot \left[\overline{u_z} \times \overline{g_t}(x,y)\right] e^{-\gamma z} \tag{8d}$$

where index t describes transverse field components, A is field amplitude coefficient, Z_F characteristic field impedance, γ propagation constant, g_t transverse vectorial structure function, and $\mathbf{u}_z$ unit vector in z direction. The structure functions are

orthogonal to each other, and in addition they will be orthonormalized:

$$\iint_A g_{t\nu} \cdot g_{t\mu} dA = \delta_{\nu\mu} \qquad (9)$$

$$where \quad \delta=1, \quad for \ \nu=\mu; \quad \delta=0 \quad for \ \nu=\mu$$

The integrals have to be evaluated over the cross section of the waveguide model. The totality of the eigen solutions and their structure functions form a complete system. An arbitrary, piecewise continuous, and transversal vector field A_t can be described by an infinite sum of the structure functions:

$$\overline{A_t} = \sum_{\nu=1}^{\infty} A_\nu \overline{g_{t\nu}} \qquad with \qquad A_\nu = \iint_A \overline{A_t} \cdot \overline{g_{t\nu}} dA \qquad (10)$$

This means that the conditions for applying the method of orthogonal series expansions are fulfilled for the waveguide model and its fields.

The forward traveling electromagnetic modes of the waveguide model can be described by an electric potential Φ_{mn} and a magnetic potential Ψ_{mn} where the indices m and n describe the field dependencies in the x and y coordinate directions, respectively:

$$\overline{E_t} = \sum_{m=0}^{\infty} \sum_{n=0}^{\infty} A_{mn}^H e^{-\gamma_{mn}^H z} (\overline{u_z} \times \nabla_t \psi_{mn}) + \sum_{m=0}^{\infty} \sum_{n=1}^{\infty} A_{mn}^E e^{-\gamma_{mn}^E z} \nabla_t \phi_{mn} \qquad (11a)$$

$$\overline{H_t} = \sum_{m=0}^{\infty} \sum_{n=0}^{\infty} \frac{A_{mn}^H}{Z_{mn}^H} e^{-\gamma_{mn}^H z} (-\nabla_t \psi_{mn}) + \sum_{m=0}^{\infty} \sum_{n=1}^{\infty} \frac{A_{mn}^E}{Z_{mn}^E} e^{-\gamma_{mn}^E z} (\overline{u_z} \times \nabla_t \phi_{mn}) \qquad (11b)$$

$$E_z = \sum_{m=0}^{\infty} \sum_{n=1}^{\infty} \frac{A_{mn}^E}{\gamma_{mn}^E} e^{-\gamma_{mn}^E z} \Delta_t \phi_{mn} \qquad (11c)$$

$$H_z = \sum_{m=0}^{\infty} \sum_{n=0}^{\infty} \frac{A_{mn}^H}{\gamma_{mn}^H Z_{mn}^H} e^{-\gamma_{mn}^H z} (-\Delta_t \psi_{mn}) \qquad (11d)$$

with

$$\gamma_{mn}^E = \gamma_{mn}^H = \alpha_{mn} + j\beta_{mn} = \sqrt{(\frac{m\pi}{w_{eff}})^2 + (\frac{n\pi}{h})^2 - \omega^2 \epsilon_0 \epsilon_{eff} \mu_0} \qquad (12a)$$

$$Z_{mn}^E = -\frac{j\gamma_{mn}^E}{\omega \epsilon_0 \epsilon_{eff}} \qquad Z_{mn}^H = \frac{j\omega\mu_0}{\gamma_{mn}^H} \qquad (12b)$$

and the potential functions

$$\phi_{mn} = \sqrt{\frac{\nu_m^E}{w_{eff} h}} \frac{1}{\sqrt{(\frac{m\pi}{w_{eff}})^2 + (\frac{n\pi}{h})^2}} \cos(\frac{m\pi}{w_{eff}} x) \sin(\frac{n\pi}{h} y) \qquad (12c)$$

$$\psi_{mn} = \frac{1}{\sqrt{w_{eff} h}} x \qquad for \quad m = n = 0 \qquad (12d)$$

$$= \sqrt{\frac{\nu_m^H}{w_{eff} h}} \frac{1}{\sqrt{(\frac{m\pi}{w_{eff}})^2 + (\frac{n\pi}{h})^2}} \sin(\frac{m\pi}{w_{eff}} x) \cos(\frac{n\pi}{h} y) \quad otherwise$$

The Neumann coefficients ν^{E}_{m} **and** ν^{H}_{m} of the TM(E) modes and the TE(H) modes are given by:

$$\nu_m^E = 2 \quad for \quad m=0,\ n\neq 0$$

$$\nu_m^E = 4 \quad for \quad m\neq 0,\ n\neq 0 \qquad (13a)$$

$$\nu_m^H = 2 \quad for \quad m\neq 0,\ n=0$$

$$\nu_m^H = 4 \qquad for \quad m \neq 0,\ n \neq 0 \qquad (13b)$$

The two different solutions in (12d) for the TEM (m=0, n=0) and TE modes can be written in one equation if for m→0 and n=0, value of ν^{H}_{m} is chosen equal to 1. An equivalent description of the backward traveling waves can also be given.

For most microstrip lines used in MIC's and MMIC's, the height h of the substrate material is small so that the electromagnetic fields of the waveguide model have no dependency on the y coordinate. Discontinuities with a change of the substrate height will not be considered here. All structures that will be analyzed are fed only with a quasi-TEM mode. As has been shown by Kompa[7], the TEM mode in discontinuity structures that are independent of the y coordinate couple only to higher-order modes that have a field distribution similar to that of the TEM mode in the coupling area. In particular, no coupling occurs between the TM(E) modes and the TEM mode and between the $TE_{mn}(H_{mn})$ modes which have y dependent electromagnetic fields ($n \neq 0$). Under these conditions only electromagnetic fields that are independent of the y coordinate can exist on the microstrip line, and as a consequence only modes of the waveguide model that are also independent of the y coordinate must be considered when modelling the microstrip discontinuities. Therefore all TM(E) modes and all $TE_{mn}(H_{mn})$ modes with $n \neq 0$ are no longer considered in the following calculations.

If in addition the field amplitudes A^{H}_{mn} and A^{E}_{mn} are replaced by wave amplitudes a_m and b_m of forward and backward traveling waves, the electromagnetic fields are

described by

$$\overline{E_t} = \sum_{m=0}^{\infty} \sqrt{Z_m}\,(a_m e^{-\gamma_m z} + b_m e^{+\gamma_m z})\,(\overline{u_z} \times \nabla_t \psi_{m0}) \qquad (14a)$$

$$\overline{H_t} = -\sum_{m=0}^{\infty} \sqrt{Y_m}\,(a_m e^{-\gamma_m z} - b_m e^{+\gamma_m z})\,\nabla_t \psi_{m0} \qquad (14b)$$

$$\overline{H_z} = -\sum_{m=1}^{\infty} \frac{\sqrt{Y_m}}{\gamma_m}\,(a_m e^{-\gamma_m z} + b_m e^{+\gamma_m z})\,\Delta_t \psi_{m0} \qquad (14c)$$

Using the potential function Ψ_{m0} as defined in (12d), the field components finally can be written as:

$$E_x = 0 \qquad (15a)$$

$$E_z = 0 \qquad (15c)$$

$$H_x = -\sum_{m=0}^{\infty} \sqrt{Y_m}\,(a_m e^{-\gamma_m z} - b_m e^{+\gamma_m z}) \sqrt{\frac{\nu_m^H}{w_{eff} h}} \cos\left(\frac{m\pi}{w_{eff}} x\right) \qquad (15d)$$

$$H_y = 0 \qquad (15e)$$

$$H_z = \sum_{m=1}^{\infty} \frac{\sqrt{Y_m}}{\gamma_m}\,(a_m e^{-\gamma_m z} + b_m e^{+\gamma_m z}) \sqrt{\frac{\nu_m^H}{w_{eff} h}}\; \frac{m\pi}{w_{eff}} \sin\left(\frac{m\pi}{w_{eff}} x\right) \qquad (15f)$$

CHAPTER 2

ASYMMETRIC SINGLE IMPEDANCE STEP

The microstrip discontinuities can be analyzed by using the waveguide model of the microstrip line along with some known mathematical methods of analyzing waveguide discontinuities or by the methods that have been developed by Kuhn [8], Wolff [7] and his research group. Five analysis methods have been derived [6]. In each method the microstrip discontinuity structure is divided into subregions, and in each subregion the electromagnetic fields are defined using complete series or integral expansions that fulfill the boundary conditions on the electric and magnetic walls. At the common interfaces between the subregions the boundary conditions are fulfilled in an integral sense, thereby defining the coupling of the field modes in the different regions. The scattering parameters of the microstrip structure can be computed if, in addition, the structure under consideration is excited only by the fundamental TEM mode. Kompa[6] suggested a method which has been used to solve the problem of finding the scattering parameters of a microstrip impedance step. For the analysis, microstrip impedance step is first replaced by an equivalent step of a waveguide model structure, and then the mode matching technique (as suggested by Kompa[6]) at the common interface is applied, using the complete series. Using this method, the results are numerical models for microstrip discontinuities that are of medium numerical expense and of good accuracy and can be used in computer-aided circuit analysis even with a desktop computer.

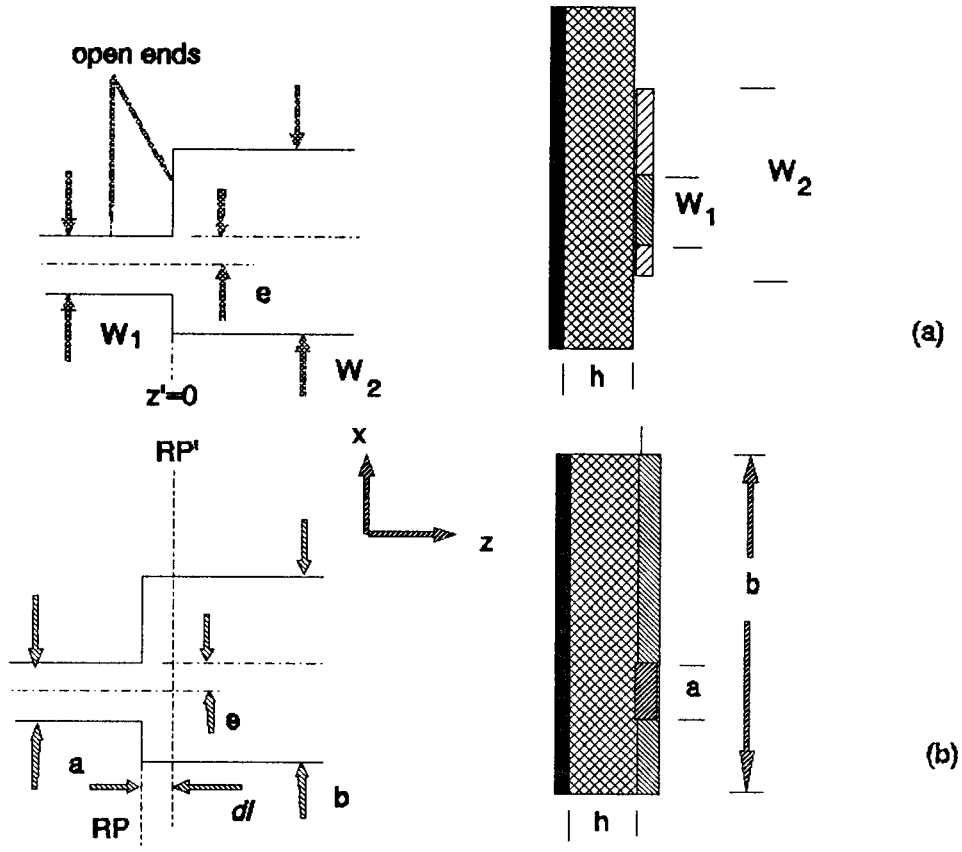

Figure 2 (a) The asymmetrical microstrip impedance step; (b) The equivalent waveguide model structure.

Figure 2 shows the original microstrip structure and the equivalent waveguide model impedance step which is divided into two field regions A and B. The widths a and b are the frequency dependent effective widths of the waveguide model, and the model is filled with a material described by the frequency dependent effective dielectric constant as discussed in the previous section. If the reference plane (RP')

of the original microstrip impedance step is at z'=0 (Figure 2a), this reference plane, because of the stray fields at the open ends of the structure is shifted to the position RP at z=0 or z'=1, figure 2b in the waveguide model. To get the correct phase information for the microstrip impedance step, this reference plane displacement must be calculated back into the original position (z'=0) after the analysis with the waveguide model. Two additional reference planes RP_A and RP_B are defined left and right from the step reference plane RP in the waveguide model structure. It is required that higher-order modes that are excited at RP be decreased to zero at RP_A and RP_B so that a scattering matrix of the fundamental mode can be defined without problems at these planes. The distances l_A and l_B of these reference planes from the plane RP are assumed to be zero in the final calculations. Under these assumptions the electromagnetic fields in region A and B are described by complete, infinite sums (discrete spectra) of eigen functions of forward and backward traveling waves [compare equations(11)-(13)].

Region A:

$$\overline{E_t^A}(z) = \sum_{m=0}^{\infty} U_m^A(z)\,(\overline{u_z}\times\nabla_t\psi_m^A) \qquad (16a)$$

$$\overline{H_t^A}(z) = \sum_{m=0}^{\infty} I_m^A(z)\,(-\nabla_t\psi_m^A) \qquad (16b)$$

with

$$\sqrt{Y_m^A}\,U_m^A(z) = a_m^A e^{-j\beta_m^A z} + b_m^A e^{j\beta^{A_m} z} \qquad (16c)$$

$$\sqrt{Z_m^A}\,I_m^A(z) = a_m^A e^{-j\beta_m^A z} - b_m^A e^{j\beta_m^A z} \qquad (16d)$$

Region B:

Considering the coordinate transformation from region A to region B, the following equations are valid for the electromagnetic fields:

$$\overline{E_t^B}(z) = \sum_{p=0}^{\infty} U_p^B(z)\,(\overline{u_z}\times\nabla_t\psi_p^B) \qquad (17a)$$

$$\overline{H_t^B}(z) = \sum_{p=0}^{\infty} I_p^B(z)\,(-\nabla_t\psi_p^B) \qquad (17b)$$

with

$$\sqrt{Y_p^B}\,U_p^B(z) = a_p^B e^{j\beta_p^B z} + b_p^B e^{-j\beta_p^B z} \qquad (17c)$$

$$\sqrt{Z_p^B}\,I_p^B(z) = a_p^B e^{j\beta_p^B z} - b_p^B e^{-j\beta_p^B z} \qquad (17d)$$

For the potential functions of region A, eqns.(11)-(13) with $w_{eff}=a$ and $n=0$ and considering the changed coordinate system are applicable:

$$\psi_m^A = \frac{1}{\sqrt{ah}}\left(x+\frac{a}{2}\right) \qquad for\ \ m=0$$

$$\psi_m^A = \sqrt{\frac{2}{ah}}\left(\frac{a}{m\pi}\right)\sin\left(\frac{m\pi}{a}x+\frac{a}{2}\right) \qquad for\ \ m\neq 0 \qquad (18a)$$

For region B, because of the coordinate transformation from region A to region B (ecentricity ε), the equations are;

$$\psi_p^B = \frac{1}{\sqrt{bh}}\left(x+\frac{b^*}{2}\right) \qquad for\ \ p=0$$

$$\psi_p^B = \sqrt{\frac{2}{bh}}\left(\frac{b}{p\pi}\right)\sin\left[\frac{p\pi}{b}\left(x + \frac{b^*}{2}\right)\right] \qquad for\ \ p\neq 0 \qquad (18b)$$

with $b^*/2 = b/2 - \varepsilon$. a_m^A, b_m^A and a_p^B, b_p^B are the normalized field (wave) amplitudes of the forward and backward traveling waves in the region A and region B, respectively. In the boundary between region A and region B the electromagnetic fields must fulfill the boundary conditions;

$$H_x^B = 0 \text{ in } A_B - A_A; \quad H_x^A = H_x^B \text{ in } A_A; \quad E_y^A = E_y^B \text{ in } A_A \qquad (19)$$

where A_A is the common boundary of the two waveguides and A_B-A_A is the magnetic wall that close the broad waveguide at the discontinuity. Because A_B-A_A is a magnetic wall, the tangential magnetic field component must vanish in it. The boundary conditions given in eqn(19) can be fulfilled only if the transverse magnetic field of region A is developed into the eigenfunctions of the region B. With this technique the amplitude coefficients I_m^B in eqn(17b) can be chosen so that the magnetic field component H_x^B vanishes on A_B-A_A and additionally H_x^A is equal to H_x^B in A_A. Conversely, the electric field component need not fulfill any special boundary condition in A_B-A_A, so the electric field components in the common boundary area A_A can be developed into the eigenfunctions of region A.

The amplitude coefficients U and I can be calculated using eqn(10) and the orthogonality relationship (eqn(9)). If eqns(17) are multiplied by ($\text{grad}_t\ U_m$) and integrated over the area A_B, the result is

$$I_P^B = \int_{A_B} H_t^B \cdot \nabla_t \psi_P^B \, dA \qquad (20)$$

Analogously, after multiplication of eqns(16) with ($\mathbf{u}_z$ x grad$_t$U$_m$) and integration over A_A, it follows that

$$U_M^A = \int_{A_A}\int E_t^A \cdot (\overline{u_z} \times \nabla_t \psi_M^A)\ dA \qquad (21)$$

If the boundary conditions are introduced into eqn(20) and (21), the remaining amplitude coefficients can be calculated:

$$I_P^B = \int_{A_A}\int H_t^A \cdot \nabla_t \psi_P^B\ dA \qquad (22)$$

$$U_M^A = \int_{A_B}\int E_t^B \cdot (\overline{u_z} \times \nabla_t \psi_M^A)\ dA \qquad (23)$$

The discontinuity problem of an asymmetrical microstrip impedance step is thus reduced to the solution of a multiple infinite system of coupled linear equations for the amplitudes of the electric and magnetic field strengths. The coefficients of the equation system are integrals over the product of the eigenfunctions of different field regions. Their evaluation gives information on the coupling between different modes in the waveguide model. In the case that the microstrip line and therefore the waveguide model are excited by a TEM mode (or an H_{m0} mode), the result is

$$U_M^A = \sum_{p=0}^{\infty} U_P^B K_{MP} \qquad I_P^B = -\sum_{m=0}^{\infty} I_m^A K_{mP} \qquad (24)$$

$$K_{00} = \sqrt{\frac{a}{b}} \qquad K_{0p} = 0 \qquad K_{0p} = \sqrt{\frac{8}{ab}}\,\frac{b}{\pi}\cos\left(\frac{p\pi}{2}\,\frac{b^*}{b}\right)\sin\left(\frac{p\pi}{2}\,\frac{a}{b}\right) \qquad (25)$$

and

$$K_{mp} = -\frac{2}{\sqrt{ab}}\,\frac{p\pi/b}{(m\pi/a)^2}\left[(-1)^m \sin\left(\frac{p\pi}{2}\left[\frac{a+b^*}{b}\right]\right) + \sin\left(\frac{p\pi}{2}\left[\frac{a-b^*}{b}\right]\right)\right]$$

$$for \quad \frac{m}{a} \neq \frac{p}{b} \qquad (26a)$$

$$K_{mp} = \sqrt{\frac{a}{b}} \cos\left[\frac{\pi}{2}\left(m - \frac{b^*}{b}p\right)\right] \qquad for \quad \frac{m}{a} = \frac{p}{b} \qquad (26b)$$

Introducing the wave amplitudes as given in eqn(16c) and (17c) into eqn(24), the equation system can be written as

$$\sqrt{Z_m^A}\,(a_M^A + b_M^A) = \sum_{p=0}^{\infty} \sqrt{Z_p^B}\, K_{Mp}\,[a_p^B + b_p^B] \qquad (27a)$$

$$\sqrt{Y_p^B}\,(a_P^B - b_P^B) = -\sum_{m=0}^{\infty} \sqrt{Y_m^A}\, K_{mP}\,[a_m^A - b_m^A] \qquad (27b)$$

with m,M,p,P = 0,1,2,..... If this equation system is rearranged so that the amplitudes b_m^A and b_p^B of the reflected waves are connected to the amplitudes a_m^A and a_p^B of the incident waves of the regions A and B, respectively, the connecting matrix is the scattering matrix:

$$\begin{vmatrix} b_0^A \\ b_1^A \\ \cdot \\ \cdot \\ \hline b_0^B \\ b_1^B \\ \cdot \\ \cdot \end{vmatrix} = \left|\begin{array}{cccc:cccc} S_{00}^{AA} & S_{01}^{AA} & \cdots & & S_{00}^{AB} & S_{01}^{AB} & \cdots & \\ S_{10}^{AA} & S_{11}^{AA} & \cdots & & S_{10}^{AB} & S_{11}^{AB} & \cdots & \\ \cdot & \cdot & & & \cdot & \cdot & & \\ \cdot & \cdot & & & \cdot & \cdot & & \\ \hline S_{00}^{BA} & S_{01}^{BA} & \cdots & & S_{00}^{BB} & S_{01}^{BB} & \cdots & \\ S_{10}^{BA} & S_{11}^{BA} & \cdots & & S_{10}^{BB} & S_{11}^{BB} & \cdots & \\ \cdot & \cdot & & & \cdot & \cdot & & \\ \cdot & \cdot & & & \cdot & \cdot & & \end{array}\right| \begin{vmatrix} a_0^A \\ a_1^A \\ \cdot \\ \cdot \\ \hline a_0^B \\ a_1^B \\ \cdot \\ \cdot \end{vmatrix} \qquad (28)$$

For the numerical computation of the scattering matrix, eqns(27) are used. the amplitude coefficients a_m^A, a_p^B of all incident waves in regions A and B are assumed

to be zero with the exception of the amplitude a_E^i (i= A or B) of one exciting (index E) mode in region A or B, respectively. Using eqn(27), the amplitudes b_m^A and b_p^B of the waves can be calculated. If, in addition, it is assumed that $a_E^i = 1$, the amplitudes b_m^A and b_p^B are equal to the elements of the scattering matrix connecting the b amplitudes with the a amplitudes as shown in eqn(28).

Results and Discussion :

Figure 3 to 5 show the typical values of the scattering parameters for microstrip step discontinuities. The assumed substrate material is RT/Duroid with the dielectric constant of $\epsilon_r = 2.32$ and a height of h = 1.57 mm. In figure 3 the reflection coefficients $|S_{11}|$ of single microstrip impedance steps from a 50Ω line to lines of lower characteristic impedances are shown. At very low frequencies the reflection coefficients can be directly calculated from the characteristic impedances: $r = (Z_2 - Z_1)/(Z_2 + Z_1)$. With increasing frequency the reflection coefficient increases until at cutoff frequency of the first higher order mode it becomes unity. The cutoff frequencies of the lines with large line width w (i.e. the lines with low characteristic impedances) are the lowest, and as a consequence the frequency dependence of the reflection coefficients of these lines is high. In figure 4, the adjoint transmission coefficients $|S_{21}|$ of the impedance steps are shown. At the cutoff frequencies the transmission coefficients are zero in agreement with the results shown in figure 3. In the case of impedance steps with one line impedance equal to 50Ω and other line impedance higher than 50Ω, the frequency dependence of the scattering parameters

$|S_{11}|$ and $|S_{21}|$ is very small. Over a large frequency range the absolute values of the scattering parameters are well described by the low frequency values, which again are determined by the characteristic impedances. The results for the symmetric junction has been compared with the results shown by Wolff [15] and found to be in good agreement which validates the algorithm.

Figure 5 shows the convergence of the results as a function of "number of modes". It can be seen that considering 8 or 10 modes is enough to get the results within acceptable accuracy. More the number of modes considered, more is the time taken by the computer to simulate the program. Thus, considering 8 modes is a good trade-off between accuracy and time, though, here, in all the results shown, 10 modes have been considered. Number of modes can be made proportional to the width of the lines resulting in faster convergence [16].

Figure 5(a) shows the dependence of d1 (the offset between the two lines) on the scattering parameters as a function of frequency. As the value of d1 increases, i.e. the offset between the two lines increases with respect to the z-axis, the scattering parameters becomes more and more frequency dependent. This property can be used effectively to make the junction more broad band, i.e., less frequency sensitive.

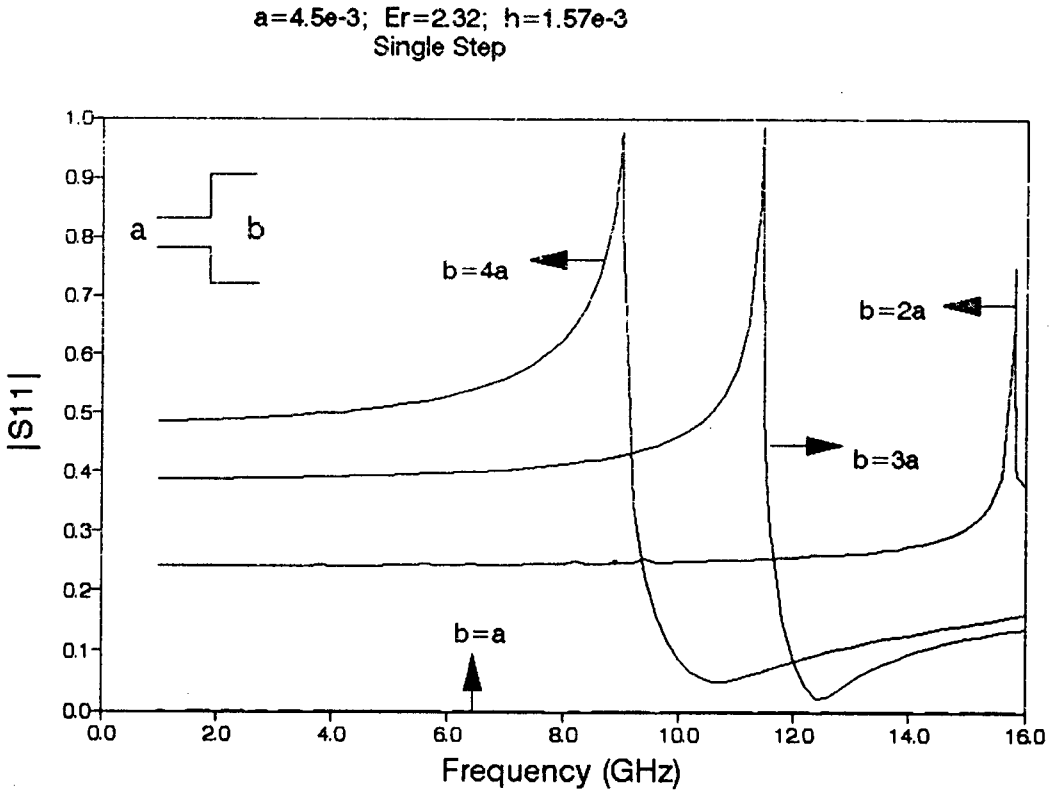

Figure 3 Reflection coefficient $|S_{11}|$ as a function of frequency for single step with output line impedance as a variable.

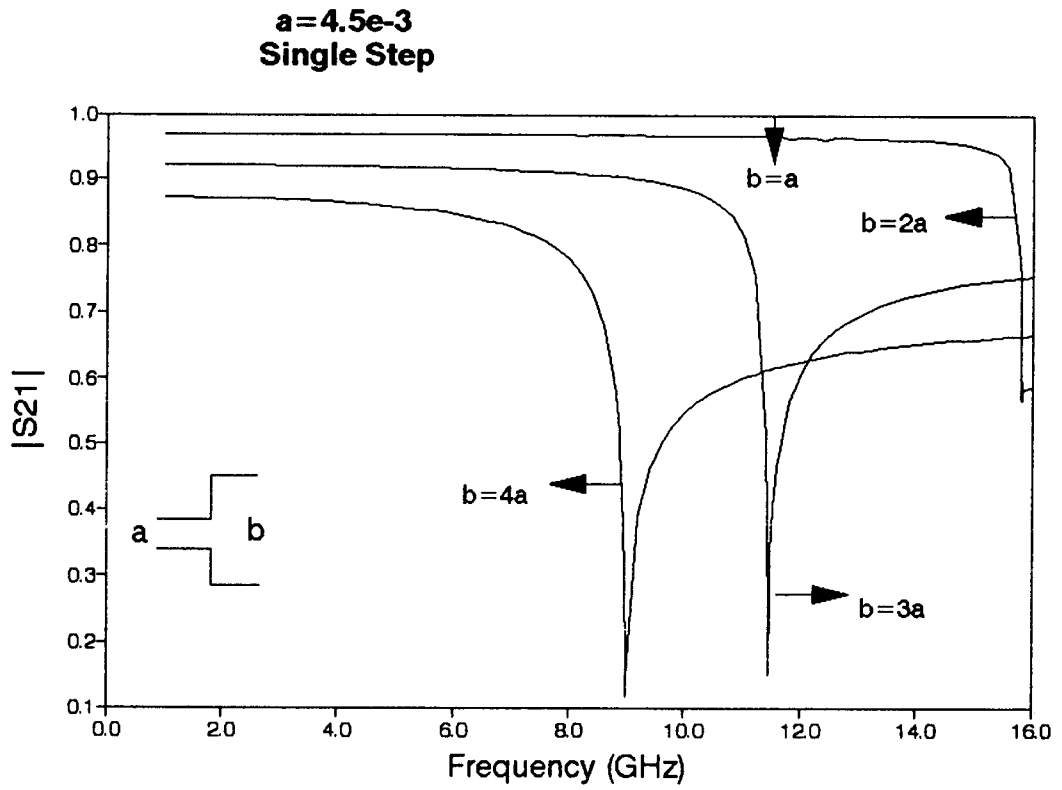

Figure 4 Transmission coefficient $|S_{21}|$ as a function of frequency for single step with output line impedance as a variable.

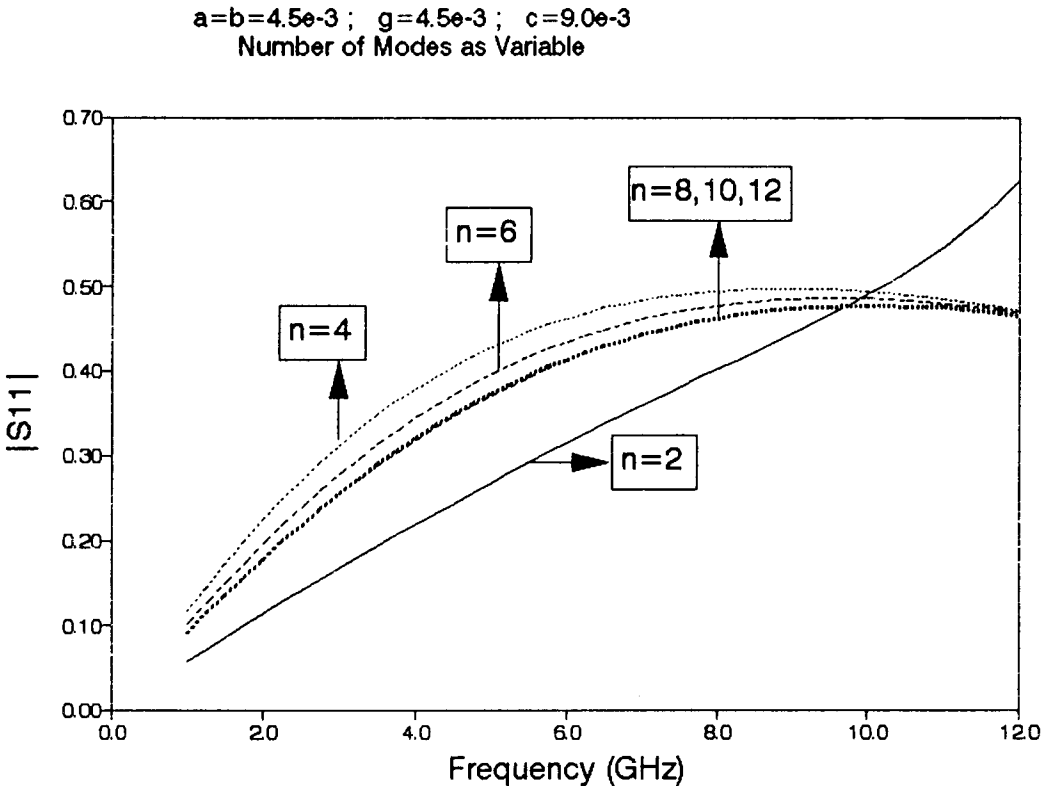

Figure 5 Reflection coefficient $|S_{11}|$ as a function of frequency for single step with number of modes as a variable.

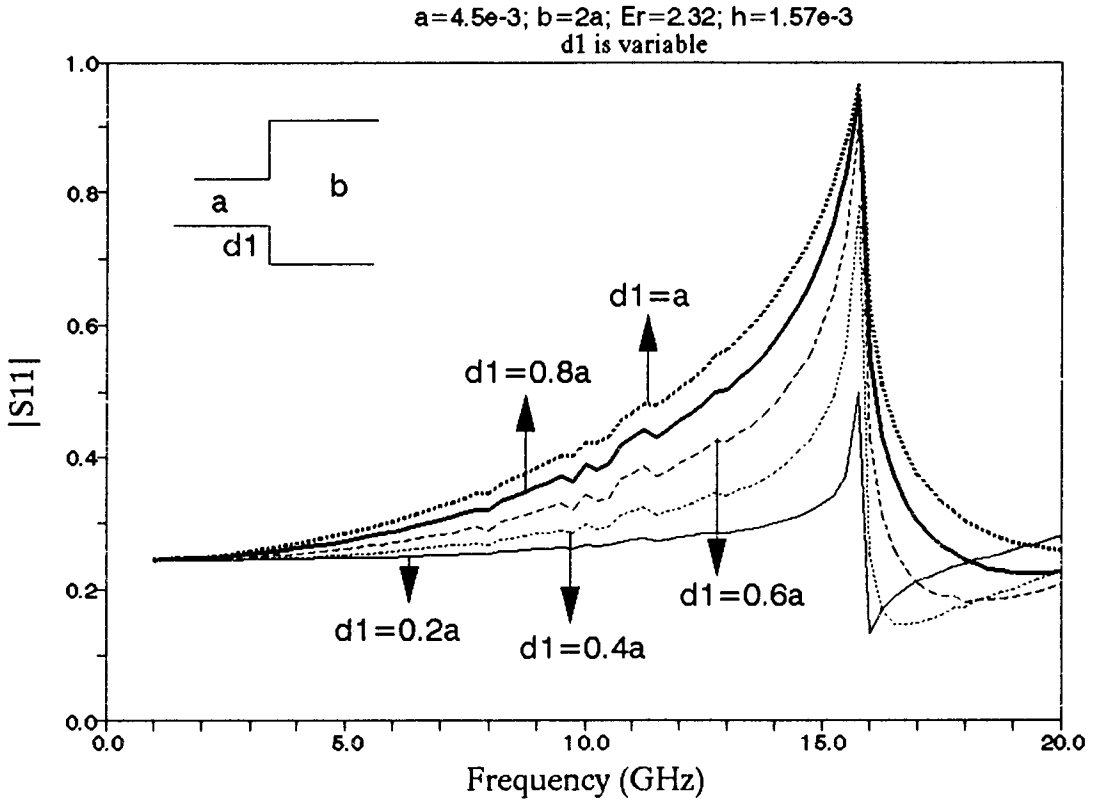

Figure 5(a) Reflection coefficient $|S_{11}|$ as a function of frequency for single step with d_1 (offset of the input line from axis) as a variable.

CHAPTER 3

INTERACTING ASYMMETRIC DOUBLE STEP

Now let us consider the case of an interacting asymmetric double step discontinuity. The asymmetric double step can be divided into three field regions, as shown in figure 6. In the figure, a and b are the frequency dependent effective widths of the two microstrip lines, and the equivalent regions of the waveguide structure are filled with a material of relative dielectric constant $\epsilon_{eff,i}$ (i = 1,2) respectively. In region III an equivalent dielectric constant, as defined in references[8,9] for a microstrip disk capacitor, is introduced, taking into account the electric stray fields only at those sides of the region where no microstrip line is connected.

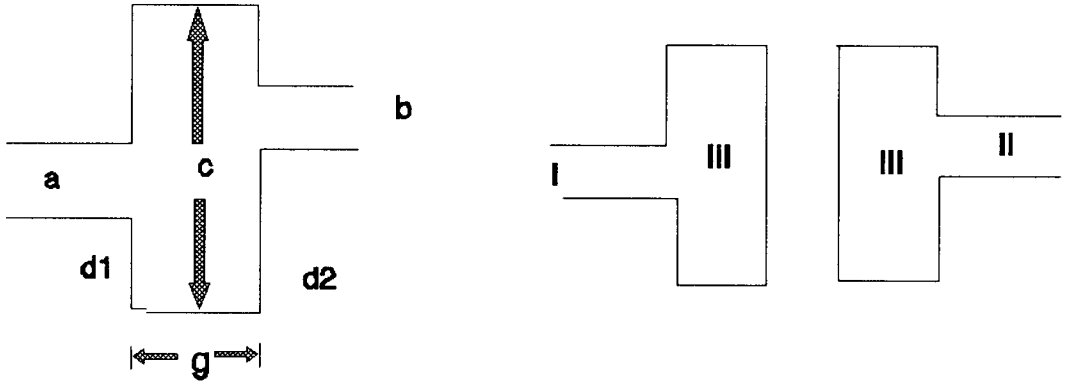

Figure 6: (a) The interacting asymmetric microstrip double step;
(b) The choice of subregions for superimposing the fields.

The boundary conditions for the electromagnetic field of region III are given by:

$$E_{\tan}^{III} = E_{\tan}^{I} \quad for \quad z=-g \quad d_1 \le x \le a+d_1 \qquad (29a)$$

$$H_{\tan}^{III} = H_{\tan}^{I} \quad for \quad z=-g \quad d_1 \le x \le a+d_1 \qquad (29b)$$

$$H_{\tan}^{III} = 0 \quad for \quad z=-g \quad 0 \le x \le d_1 \quad and \quad a+d_1 \le x \le c \qquad (29c)$$

$$E_{\tan}^{III} = E_{\tan}^{II} \quad for \quad z=0 \quad d_2 \le x \le b+d_2 \qquad (30a)$$

$$H_{\tan}^{III} = H_{\tan}^{II} \quad for \quad z=0 \quad d_2 \le x \le b+d_2 \qquad (30b)$$

$$H_{\tan}^{III} = 0 \quad for \quad z=0 \quad 0 \le x \le d_2 \quad and \quad b+d_2 \le x \le c \qquad (30c)$$

Considering the position of the two waveguides with respect to the coordinate system introduced in figure 6, the transversal field components of the field regions I and II can be described by:

$$E_y^I = \sum_{K=0}^{\infty} \sqrt{Z_K^I} \left(a_K^I e^{-j\beta_K^I(z+g)} + b_K^I e^{j\beta_K^I(z+g)}\right) \sqrt{\frac{\nu_K}{ah}} \cos\left(\frac{k\pi}{a}(x-d_1)\right) \qquad (31a)$$

$$H_x^I = -\sum_{K=0}^{\infty} \sqrt{Y_K^I} \left(a_K^I e^{-j\beta_K^I(z+g)} - b_K^I e^{j\beta_K^I(z+g)}\right) \sqrt{\frac{\nu_K}{ah}} \cos\left(\frac{k\pi}{a}(x-d_1)\right) \qquad (31b)$$

$$E_y^{II} = \sum_{m=0}^{\infty} \sqrt{Z_m^{II}} \left(a_m^{II} e^{j\beta_m^{II} z} + b_m^{II} e^{-j\beta_m^{II} z}\right) \sqrt{\frac{\nu_m}{bh}} \cos\left(\frac{m\pi}{b}(x-d_2)\right) \qquad (31c)$$

$$H_x^{II} = \sum_{m=0}^{\infty} \sqrt{Y_m^{II}} \left(a_m^{II} e^{j\beta_m^{II} z} - b_m^{II} e^{-j\beta_m^{II} z}\right) \sqrt{\frac{\nu_m}{bh}} \cos\left(\frac{m\pi}{b}(x-d_2)\right) \qquad (31d)$$

$$E_y^{IIIa} = \sum_{K=0}^{\infty} \sqrt{Z_K^{III}}\ C_K^{IIIa} \cos(\beta_K^{III} z) \sqrt{\frac{\nu_K}{ch}} \cos(\frac{K\pi}{c} x) \qquad (32a)$$

$$H_x^{IIIa} = j\sum_{K=0}^{\infty} \sqrt{Y_K^{III}}\ C_K^{IIIa} \sin(\beta_K^{III} z) \sqrt{\frac{\nu_K}{ch}} \cos(\frac{K\pi}{c} x) \qquad (32b)$$

$$E_y^{IIIb} = \sum_{m=0}^{\infty} \sqrt{Z_m^{III}}\ C_m^{IIIb} \cos(\beta_m^{III}(z+g)) \sqrt{\frac{\nu_m}{ch}} \cos(\frac{m\pi}{c} x) \qquad (32c)$$

$$H_x^{IIIb} = j\sum_{m=0}^{\infty} \sqrt{Y_m^{III}}\ C_m^{IIIb} \sin(\beta_m^{III}(z+g)) \sqrt{\frac{\nu_m}{ch}} \cos(\frac{m\pi}{c} x) \qquad (32d)$$

The phase constant β^I is the phase constant of region I (or β^{II} for region II) calculated with the equivalent dielectric constant of region III instead of ϵ_{eff} of region I.

Kuhn's method [8] is of great advantage in the sense that the magnetic fields of the region I and II can be matched to the magnetic field of region III separately because the structures that are superimposed (figure 6b) at each reference plane have only one open boundary. The remaining reference planes of the substructures are closed by magnetic walls so that the magnetic field strengths vanish here. The relationships between the fields of region I and III^a and that of II and III^b have to be determined by a normal mode-matching process. At the I and III^a interface this leads to:

$$j\sqrt{Y_K^{III}}\ C_K^{IIIa} \sin(\beta_K^{III} g) = \sum_{N=0}^{\infty} \sqrt{Y_N^I}\,(a_N^I - b_N^I)\ K_1^{N,K} \qquad (33a)$$

where

$$K_1^{N,K} = \frac{1}{h}\sqrt{\frac{\nu_K \nu_N}{ca}} \int_{z=-g}\int \cos(\frac{K\pi}{c} x) \cos(\frac{N\pi}{a}(x-d_1))\, dxdy \qquad (33b)$$

and is known as coupling integral.

Similarly, at the interface of region II and III, the result is:

$$j\sqrt{Y_M^{III}}\; C_M^{IIIb}\sin(\beta_M^{III} g) = \sum_{P=0}^{\infty}\sqrt{Y_P^{II}}\,(a_P^{II} - b_P^{II})\; K_2^{P,M} \qquad (34a)$$

where

$$K_2^{P,M} = \frac{1}{h}\sqrt{\frac{\nu_M \nu_P}{cb}}\int_{z=0}\int \cos\left(\frac{M\pi}{c}x\right)\cos\left(\frac{P\pi}{b}(x-d_2)\right)dxdy \qquad (34b)$$

Now the magnetic fields of the subregions are matched. If now the total electromagnetic field is calculated, the field solutions (32), taking into account equations (33) and (34) and the electric field strengths of waveguides I and II and the total electric field in the connecting field region III are additionally matched at the reference planes. So the boundary conditions at the boundary between region I and III that must be fulfilled by the fields is

$$E_{\tan}^{I}\big|_{z=-g} = E_{\tan}^{IIIa}\big|_{z=-g} + E_{\tan}^{IIIb}\big|_{z=-g} \qquad (35)$$

Similarly, applying the boundary condition at the boundary between regions II and III gives

$$E_{\tan}^{II}\big|_{z=0} = E_{\tan}^{IIIa}\big|_{z=0} + E_{\tan}^{IIIb}\big|_{z=0} \qquad (36)$$

Using equations 31-34 and doing some mathematics (see Appendix 'A'), we finally get;

$$(a_N^I + b_N^I) = \sum_{P=0}^{\infty}\left[\,(a_P^I - b_P^I)\,A_1^{P,N} + (a_P^{II} - b_P^{II})\,B_2^{P,N}\right] \qquad (37)$$

$$(a_N^{II} + b_N^{II}) = \sum_{P=0}^{\infty}\left[\,(a_P^I - b_P^I)\,B_1^{P,N} + (a_P^{II} - b_P^{II})\,A_2^{P,N}\right] \qquad (38)$$

where

$$A_i^{P,N} = -j\sum_{K=0}^{\infty} \frac{Z_K^{III}}{\sqrt{Z_N^i Z_P^i}} K_i^{P,K} K_i^{N,K} \cot(\beta_K^{III} g) \qquad (39)$$

$$B_i^{P,N} = -j\sum_{K=0}^{\infty} \frac{Z_K^{III}}{\sqrt{Z_N^{i'} Z_P^i}} \frac{K_i^{P,K} K_{i'}^{N,K}}{\sin(\beta_K^{III} g)} \qquad (40)$$

(i=1 or 2 and i'=1 for i=2 & i'=2 for i=1)

Results and Discussion :

Figure 7-9 show the frequency dependent transmission characteristics of typical double step discontinuities computed by the mode-matching technique as explained above. In this case the input and output lines are both 50Ω (i.e. width w = 0.0045m, ϵ_r=2.32 and height of the substrate h=1.57mm for figure 7 and w=73.1e-6m, h=100e-6m and ϵ_r=13 for figures 8-9) but middle line has an impedance varying from 50Ω to lower values. At 50Ω, as is expected, reflection coefficient is zero, but as the impedance of middle line increases, the reflection coefficient becomes more and more frequency sensitive. It can be seen from figure 7 that for c=5a and 6a plots there are two frequencies when the reflection coefficient becomes unity. This result is because at lower frequency the first higher order mode gets excited and then at second peak the next higher order mode gets excited. Figure 8 shows the similar results for the microstrip line with GaAs as substrate (w=73.1e-06m, h=1e-04m, and ϵ_r=13.0). From figure 9 we see that if the input, output and middle lines are aligned

at lower end (i.e. d_1 and d_2 are zero) then scattering parameters (reflection as well as transmission coefficients) are not very dependent on frequency and higher order modes do not get excited until very high frequency.

Figure 10 shows the effect of a double step when the input middle and output lines are of different characteristic impedances. Here, the input line has been kept at an impedance of 50Ω, while the middle line has width equal to three times that of the input line. The output line width is varied from one third the width of the input line to twice its value. It can be seen that at higher characteristic impedances of the output line ($w_{output} < w_{input}$), the reflection coefficient $|S_{11}|$ (and thus the transmission coefficient $|S_{21}|$) of this double step is more frequency dependent. As the impedance of the output line is decreased, $|S_{11}|$ becomes more and more frequency insensitive until the characteristic impedance of this output line becomes equal to that of the middle line, where it behaves exactly like the single step (see figure 11 for the plot of b=2a) (as expected). As the impedance of output line is increased further, the scattering parameter $|S_{11}|$ behaves sinusoidally at frequencies below that of the excitation of the first higher order mode. At higher frequencies, it is very sensitive to frequency. Figure 12-13 shows the behavior of the scattering parameter when the substrate is GaAs instead of RT/Duroid. When d_1 and d_2 are kept equal to zero, we see that (figure 12) the scattering parameters remains insensitive to frequency as was discussed above. Figure 13 is similar to figure 10 except that the parameters changes due to changes in ϵ_r to make the input line as 50Ω.

Figure 14(and 15) show dependence of d1 (d2) on scattering parameters as a function of frequency. When d1 = d2 = 0, difference in width of middle line, with input and output lines having same characteristic impedance, makes system more frequency sensitive. When the input line (output line) goes off the axis of output line (input line), it can be seen that higher order modes get excited which takes $|S_{11}|$ to unity at a particular frequency depending on the impedance of the input (output) and middle line (keeping output line impedance equal to the input line impedance). As one goes on increasing d1 (d2) the frequency of the excitation of the first higher order mode keeps on decreasing. This shift in frequency of the excitation of the first higher order mode becomes much more significant if we take the case of a microstrip line with GaAs as a substrate rather than RT/Duroid (figure 16). Figure 17 also shows some very interesting results. Here the dependence of the length of the middle line on the scattering parameter is shown as a function of frequency. It can be seen that as the length of the middle step is increased, $|S_{11}|$ becomes more and more frequency sensitive. The most interesting feature to note here is the frequency of excitation of the first higher order mode. It can be seen that the frequency of excitation of the first higher order mode is independent of the length of the middle line, but other higher order modes' excitation frequency depends on the middle line's length. Moreover, it can be seen that this cut-off frequency is the same as the cut-off frequency of the single step keeping all other parameters same (figure 3: plot for b = 3a). These results can effectively be used in designing filters of different types and for a desired frequency range, e.g. band pass, band reject, high pass, low pass.

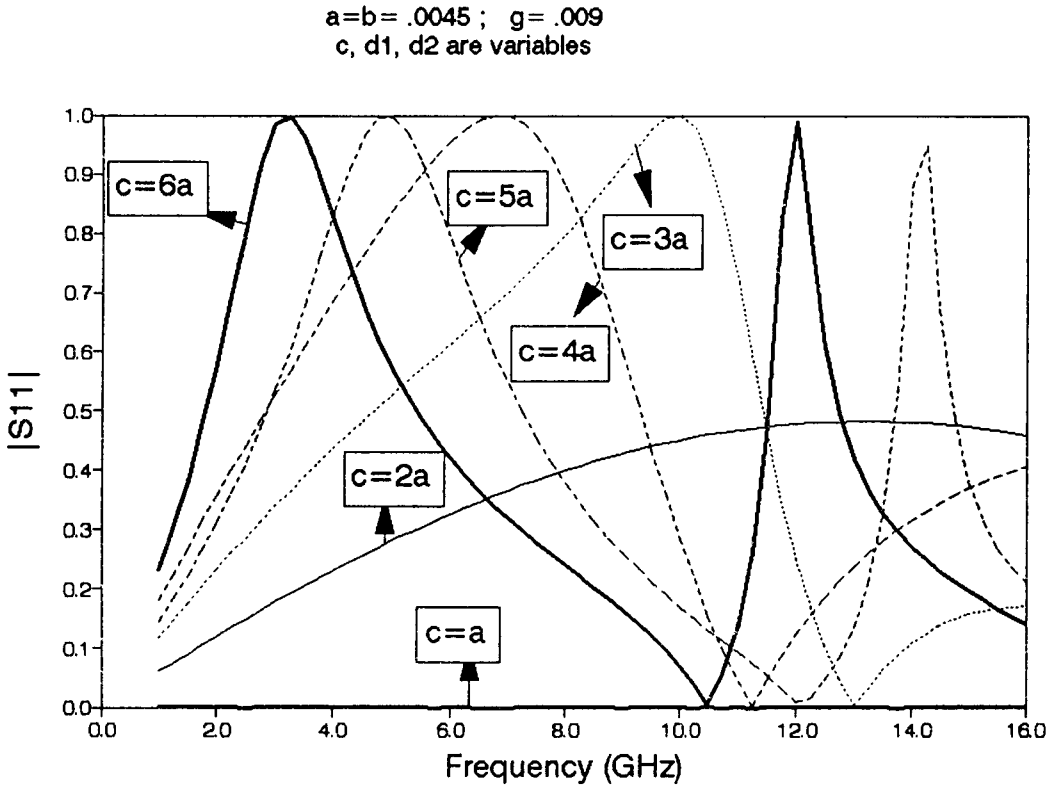

Figure 7 $|S_{11}|$ as a function of frequency for double step with c, d_1 and d_2 as variables.

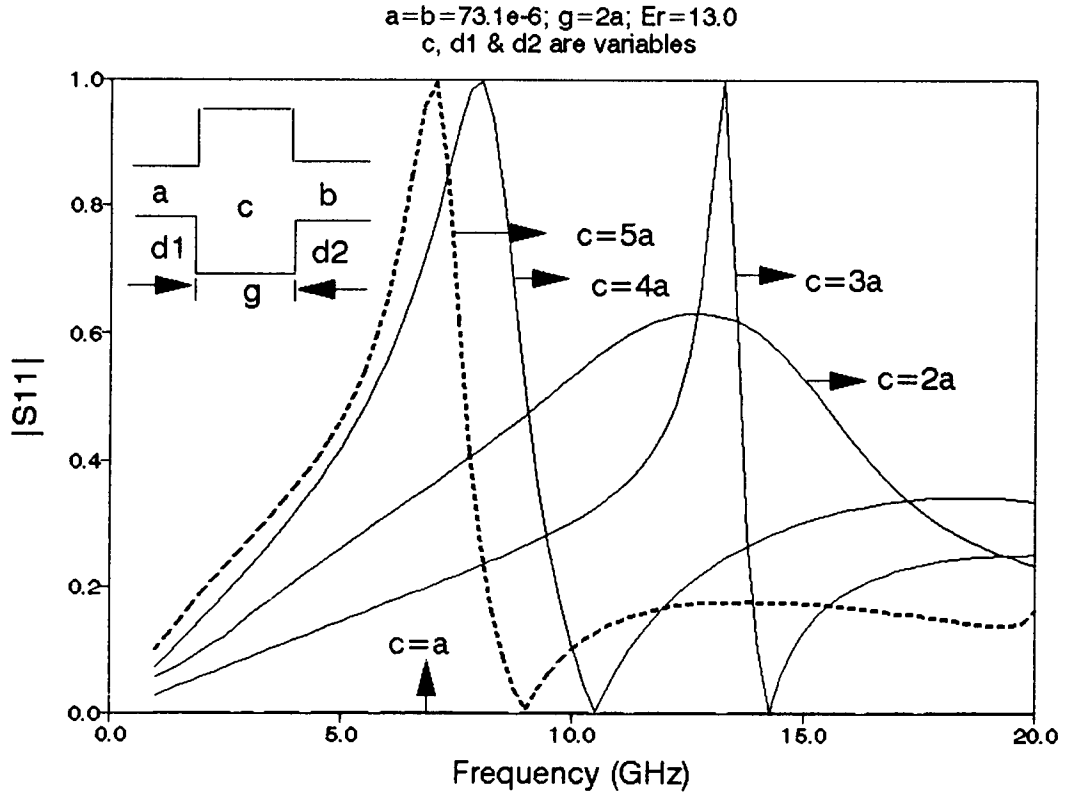

Figure 8 $|S_{11}|$ as a function of frequency for double step with c, d_1 and d_2 as variables.

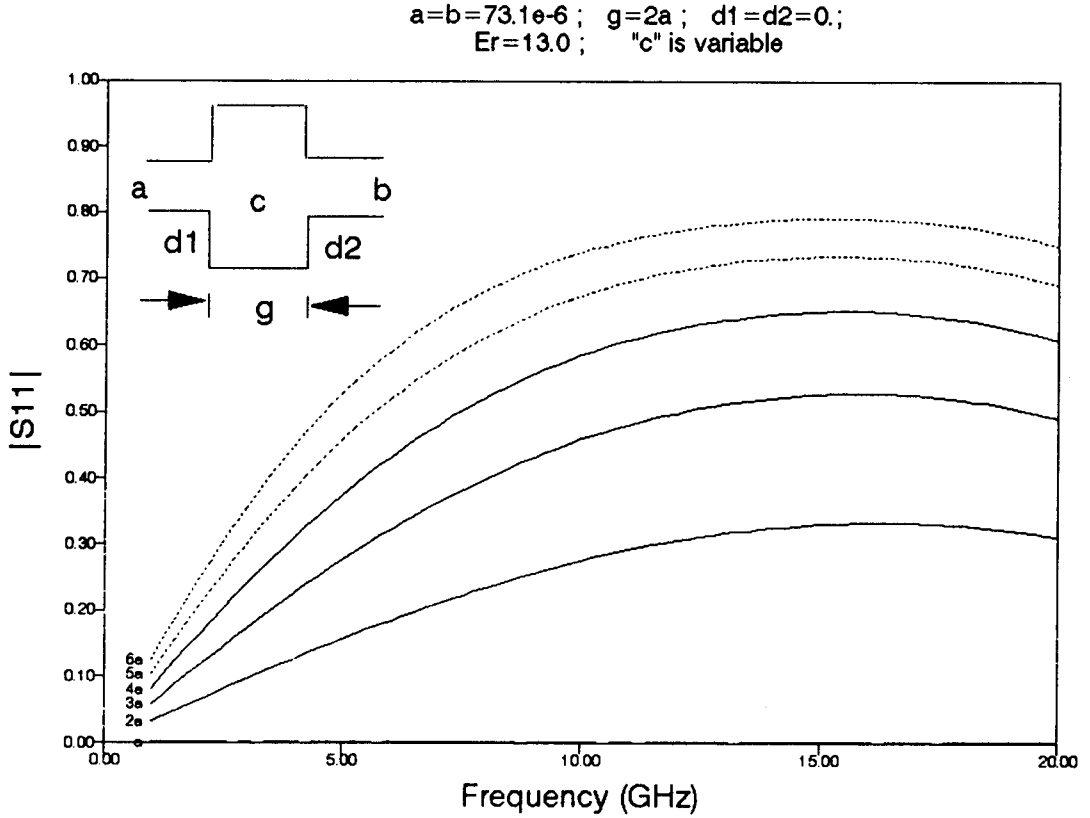

Figure 9 $|S_{11}|$ as a function of frequency for double step with c as a variable.

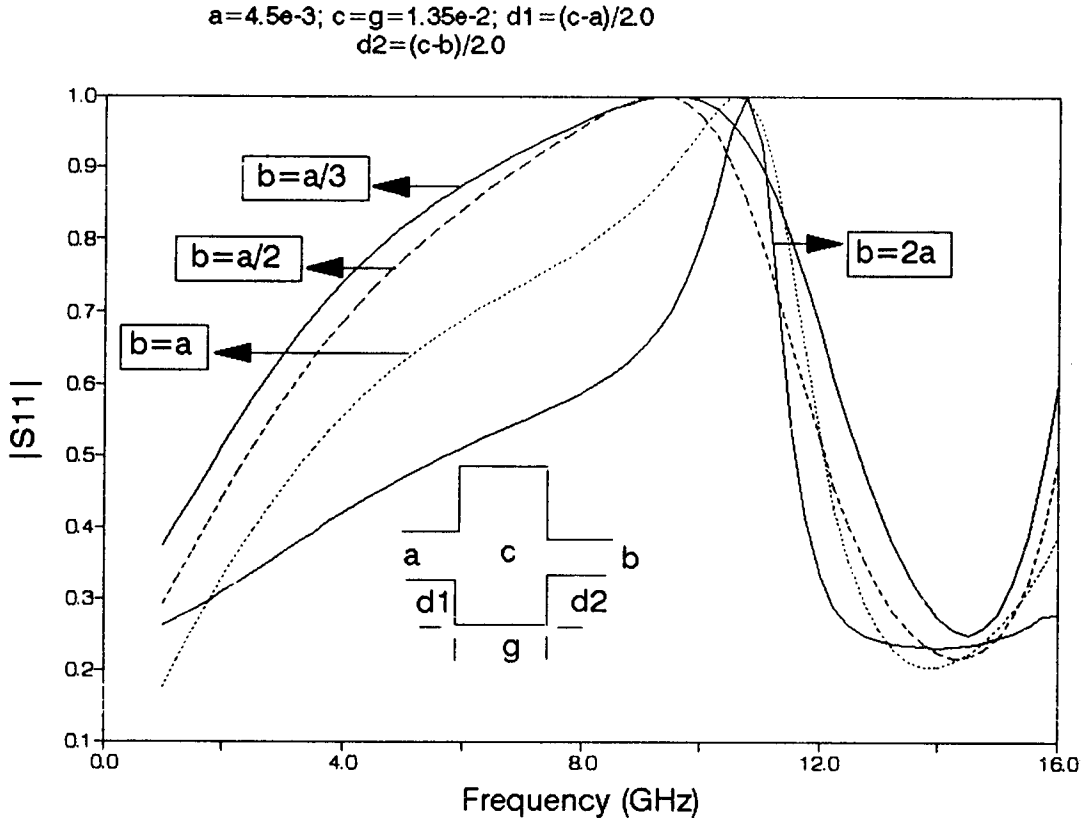

Figure 10 $|S_{11}|$ as a function of frequency for double step with b as a variable.

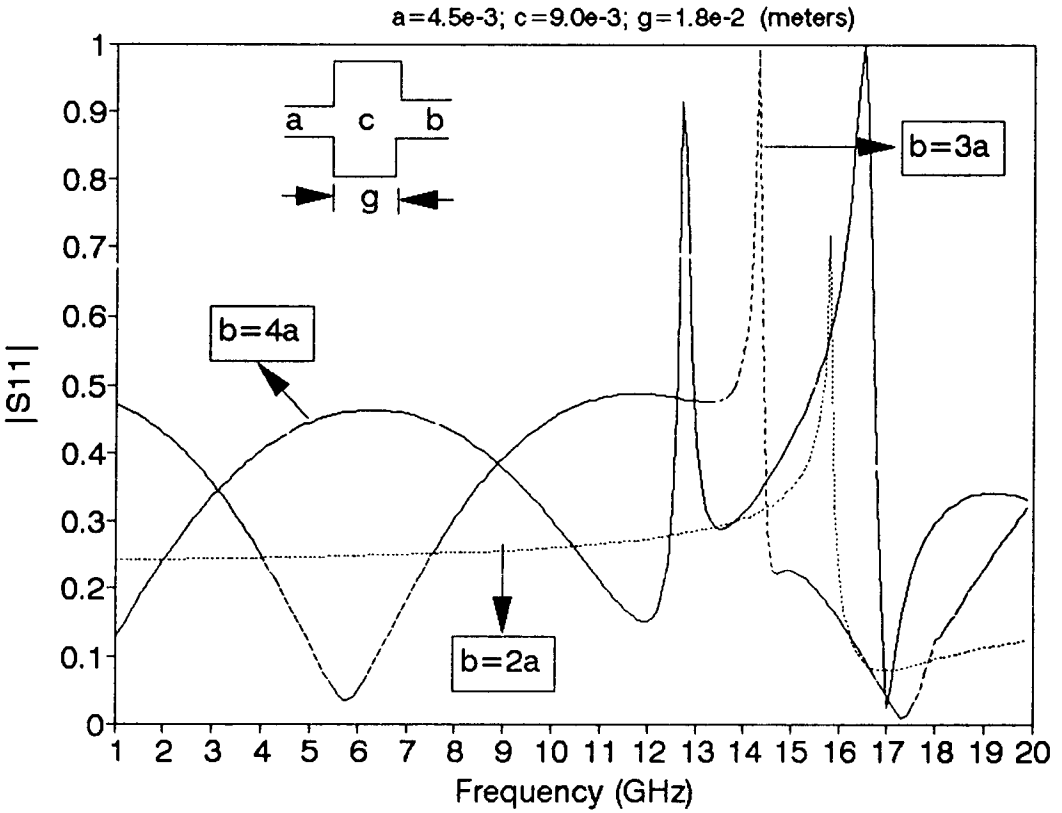

Figure 11 $|S_{11}|$ as a function of frequency for double step with b as a variable.

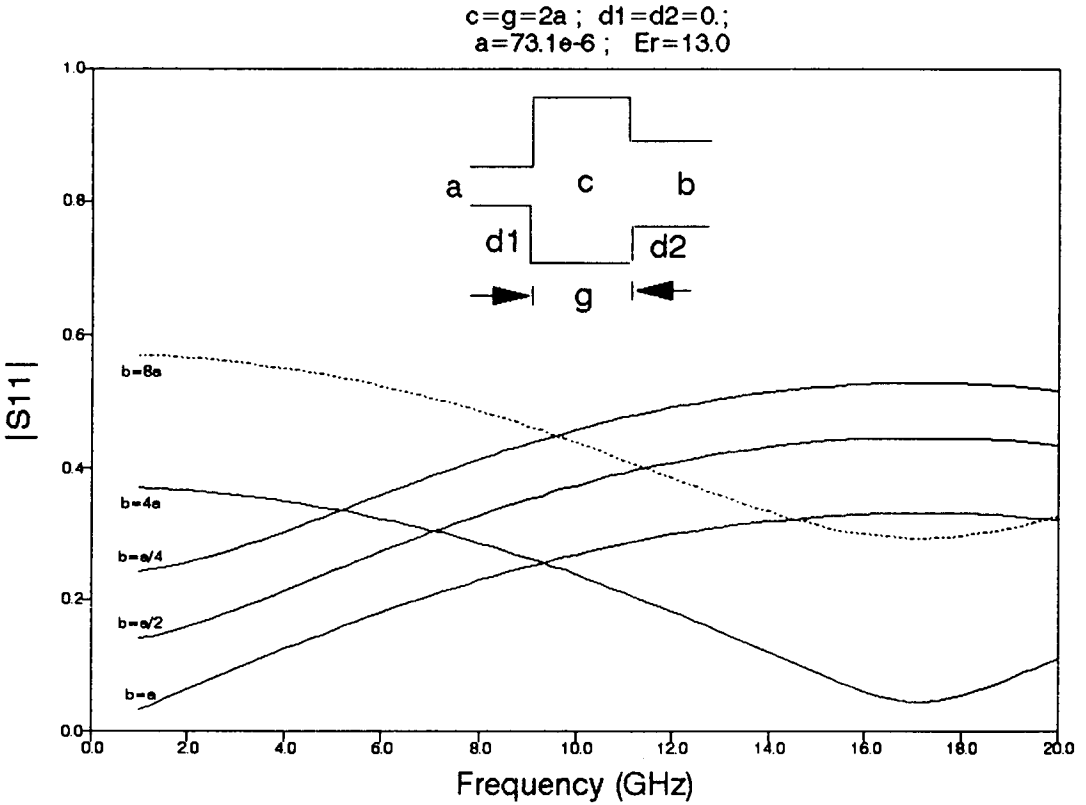

Figure 12 $|S_{11}|$ as a function of frequency for double step with b as a variable.

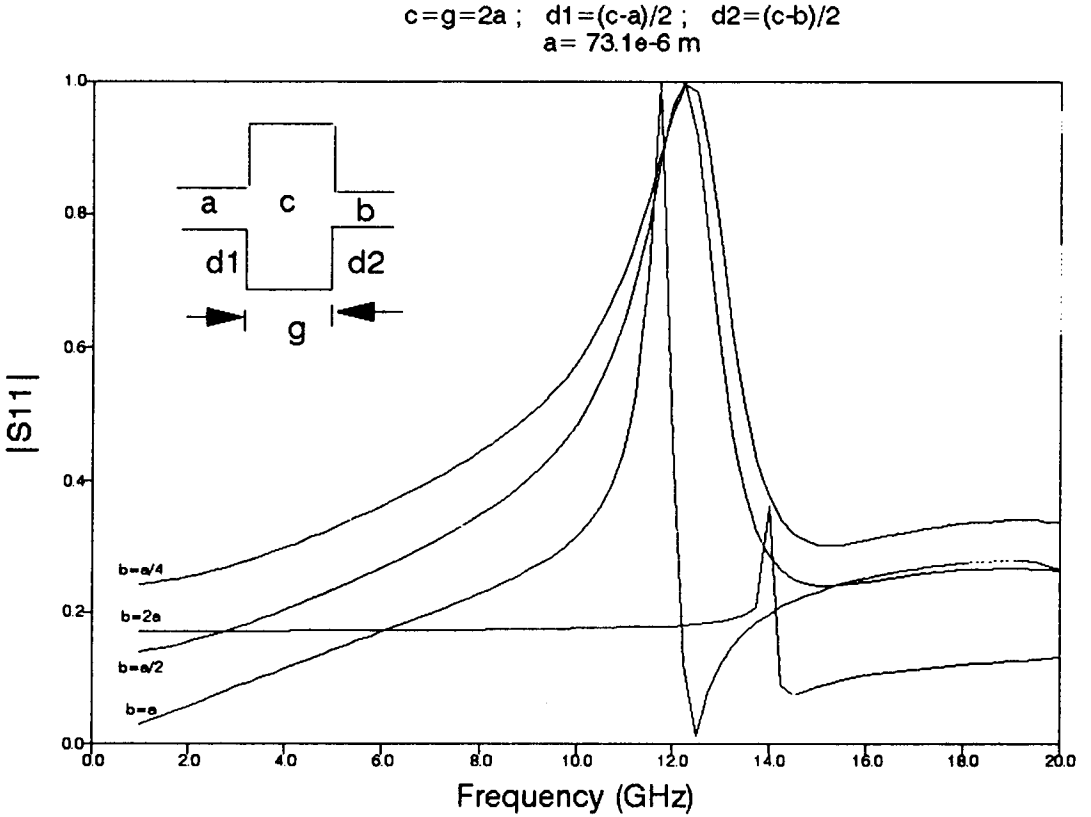

Figure 13 $|S_{11}|$ as a function of frequency for double step with b as a variable.

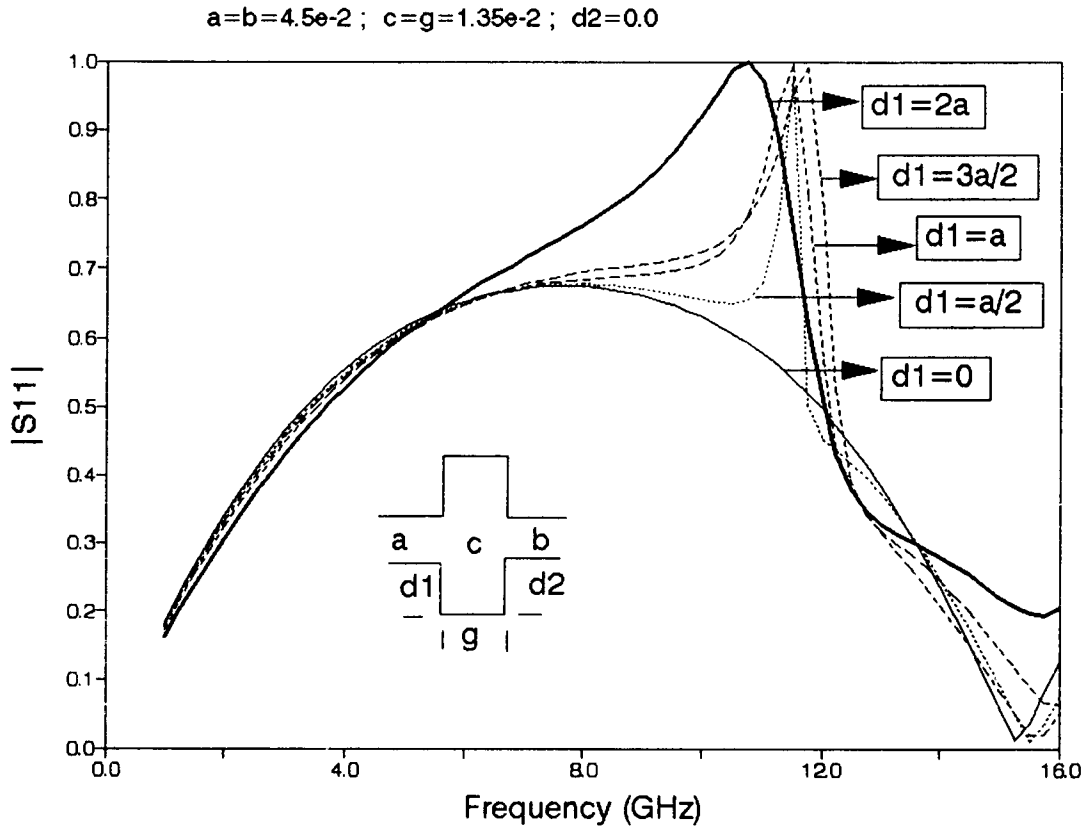

Figure 14 $|S_{11}|$ as a function of frequency for double step with d_1 as variable.

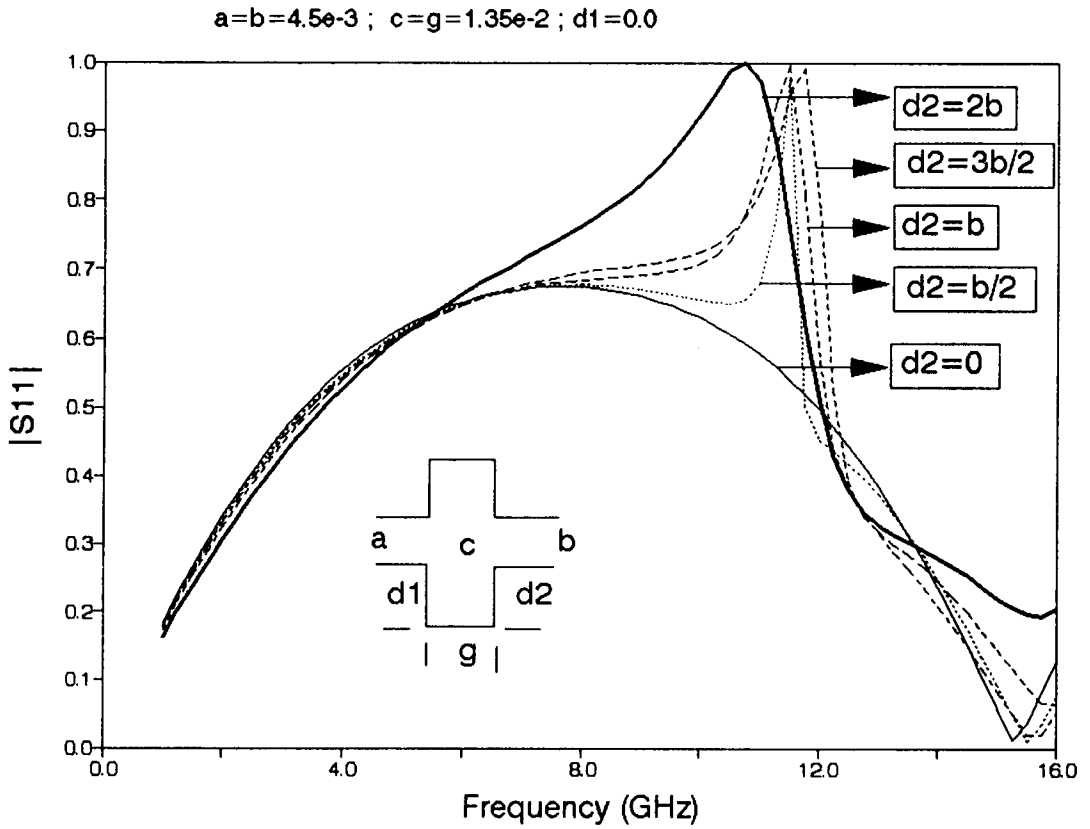

Figure 15 $|S_{11}|$ as a function of frequency for double step with d_2 as variable

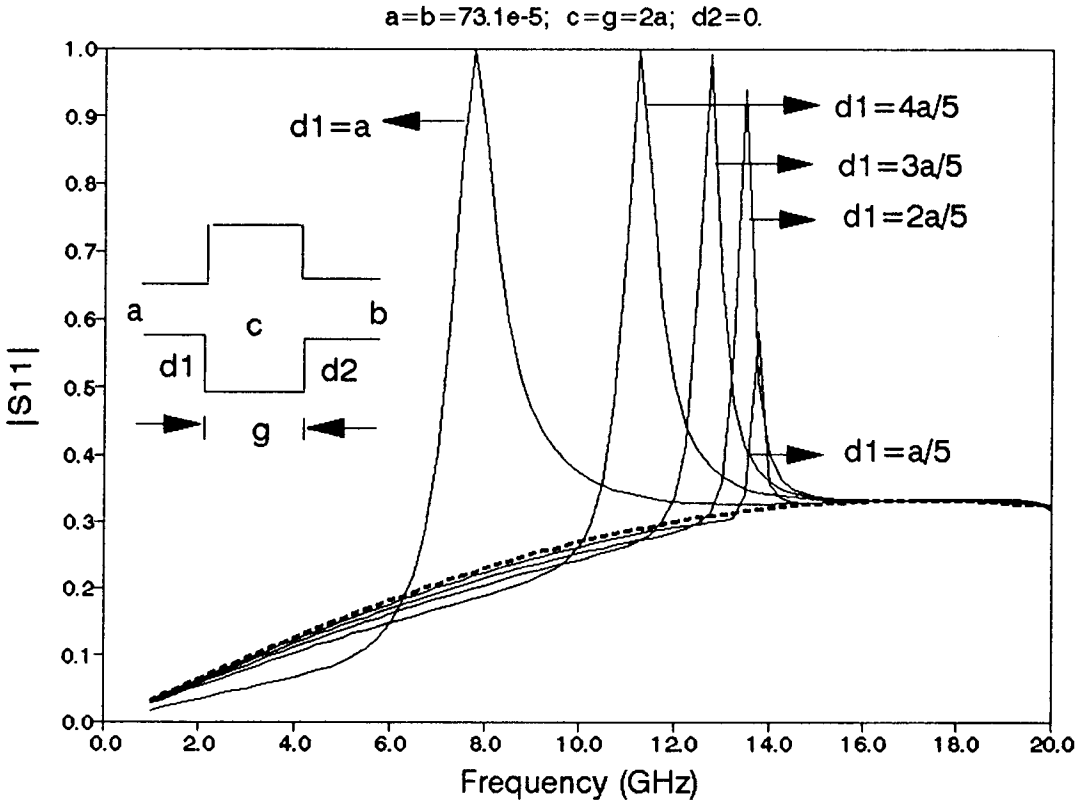

Figure 16 $|S_{11}|$ as a function of frequency for double step with d_1 as variable.

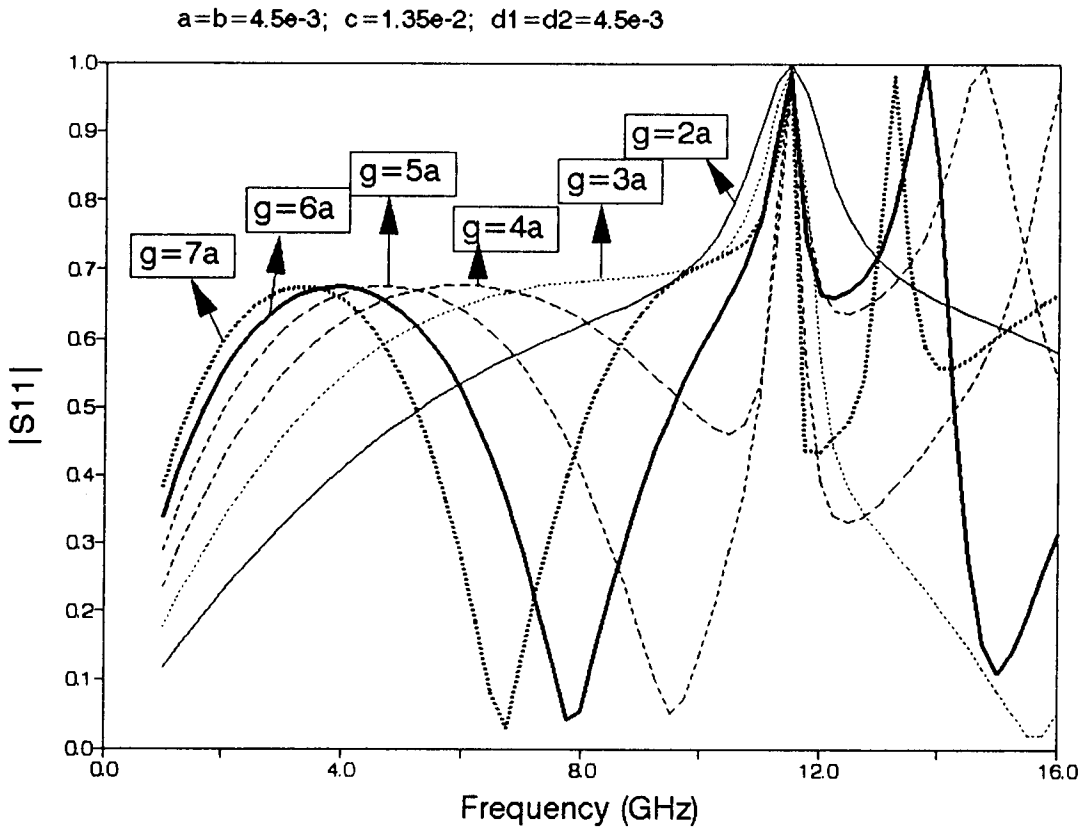

Figure 17 $|S_{11}|$ as a function of frequency for double step with g as a variable.

CHAPTER 4

INTERACTING ASYMMETRIC DOUBLE STEP WITH MULTIPLE OUTPUT LINES

In the previous chapter interacting asymmetric double step discontinuities with single output line were discussed. In the present chapter, the effect of this type of discontinuity in the presence of more than one output line is studied. The objective is to investigate the application of such structures as useful multiport circuits such as power dividers and combiners. Again the asymmetric double step can be divided into (n+2) regions, where n is the number of output lines (see figure 18). In figure 18, a is the frequency dependent effective width of the input line, where as b_1, b_2,..,b_n are the frequency dependent effective width of the output lines. The boundary conditions for the electromagnetic field of region III are given by :

$$E_{\tan}^{III} = E_{\tan}^{I} \quad for \quad z=-g \quad d_1 \le x \le a+d_1 \qquad (41a)$$

$$H_{\tan}^{III} = H_{\tan}^{I} \quad for \quad z=-g \quad d_1 \le x \le a+d_1 \qquad (41b)$$

$$H_{\tan}^{III} = 0 \quad for \quad z=-g \quad 0 \le x \le d_1 \quad and \quad a+d_1 \le x \le c \qquad (41c)$$

$$E_{\tan}^{III} = E_{\tan}^{II_1} \quad for \quad z=0 \quad d_2(1) \le x \le b_1+d_2(1) \qquad (42a)$$

$$H_{\tan}^{III} = H_{\tan}^{II_1} \quad for \quad z=0 \quad d_2(1) \le x \le b_1+d_2(1) \qquad (42b)$$

$$H_{\tan}^{III} = 0 \quad for \quad z=0 \quad 0 \le x \le d_2(1) \quad and \quad b_1+d_2(1) \le x \le c \qquad (42c)$$

$$E_{\tan}^{III} = E_{\tan}^{II_n} \quad for \quad z=0 \quad d_2(n) \le x \le b_1+d_2(n) \qquad (43a)$$

$$H_{\tan}^{III} = H_{\tan}^{II_n} \quad for \quad z=0 \quad d_2(n) \le x \le b+d_2(n) \qquad (43b)$$

$$H_{\tan}^{III} = 0 \quad for \quad z=0 \quad 0 \le x \le d_{n+1} \quad and \quad b+d_2(n) \le x \le c \qquad (43c)$$

where subscript I, II and III stands for the input, output and middle lines, d_1, $d_2(1)$,..., $d_2(n)$ are the offset of the input and output lines from the z-axis. Considering the position of the waveguides with respect to the coordinate system introduced in figure 18, the transversal field components of the field regions I and II can be described by

$$E_y^I = \sum_{K=0}^{\infty} \sqrt{Z_K^I} \left(a_K^I e^{-j\beta_K^I(z+g)} + b_K^I e^{j\beta_K^I(z+g)}\right) \sqrt{\frac{\nu_K}{ah}} \cos\left(\frac{k\pi}{a}(x-d_1)\right) \qquad (44a)$$

$$H_x^I = -\sum_{K=0}^{\infty} \sqrt{Y_K^I} \left(a_K^I e^{-j\beta_K^I(z+g)} - b_K^I e^{j\beta_K^I(z+g)}\right) \sqrt{\frac{\nu_K}{ah}} \cos\left(\frac{k\pi}{a}(x-d_1)\right) \qquad (44b)$$

$$E_y^{II_1} = \sum_{m=0}^{\infty} \sqrt{Z_m^{II_1}} \left(a_m^{II_1} e^{j\beta_m^{II_1} z} + b_m^{II_1} e^{-j\beta_m^{II_1} z}\right) \sqrt{\frac{\nu_m}{b_1 h}} \cos\left(\frac{m\pi}{b_1}(x-d_2(1))\right) \qquad (44c$$

$$H_x^{II_1} = \sum_{m=0}^{\infty} \sqrt{Y_m^{II_1}} \left(a_m^{II_1} e^{j\beta_m^{II_1} z} - b_m^{II_1} e^{-j\beta_m^{II_1} z}\right) \sqrt{\frac{\nu_m}{b_1 h}} \cos\left(\frac{m\pi}{b_1}(x-d_2(1))\right) \qquad (44$$

$$E_y^{II_n} = \sum_{m=0}^{\infty} \sqrt{Z_m^{II_n}} \left(a_m^{II_n} e^{j\beta_m^{II_n} z} + b_m^{II_n} e^{-j\beta_m^{II_n} z}\right) \sqrt{\frac{\nu_m}{b_n h}} \cos\left(\frac{m\pi}{b_n}(x-d_2(n))\right) \qquad (44e$$

$$H_x^{II_n} = \sum_{m=0}^{\infty} \sqrt{Y_m^{II_n}} \left(a_m^{II_n} e^{j\beta_m^{II_n} z} - b_m^{II_n} e^{-j\beta_m^{II_n} z}\right) \sqrt{\frac{\nu_m}{b_n h}} \cos\left(\frac{m\pi}{b_n}(x-d_2(n))\right) \qquad (44f$$

$$E_y^{IIIa} = \sum_{K=0}^{\infty} \sqrt{Z_K^{III}}\ C_K^{IIIa} \cos(\beta_K^{III} z) \sqrt{\frac{\nu_K}{ch}} \cos\left(\frac{K\pi}{c} x\right) \qquad (45a)$$

$$H_x^{IIIa} = j\sum_{K=0}^{\infty} \sqrt{Y_K^{III}}\ C_K^{IIIa} \sin(\beta_K^{III} z) \sqrt{\frac{\nu_K}{ch}} \cos\left(\frac{K\pi}{c} x\right) \qquad (45b)$$

$$E_y^{IIIb_1} = \sum_{m=0}^{\infty} \sqrt{Z_m^{III}}\ C_m^{IIIb_1} \cos(\beta_m^{III}(z+g)) \sqrt{\frac{\nu_m}{ch}} \cos\left(\frac{m\pi}{c} x\right) \qquad (45c)$$

$$H_x^{IIIb_1} = j\sum_{m=0}^{\infty} \sqrt{Y_m^{III}}\ C_m^{IIIb_1} \sin(\beta_m^{III}(z+g)) \sqrt{\frac{\nu_m}{ch}} \cos\left(\frac{m\pi}{c} x\right) \qquad (45d)$$

$$E_y^{IIIb_n} = \sum_{m=0}^{\infty} \sqrt{Z_m^{III}}\ C_m^{IIIb_n} \cos(\beta_m^{III}(z+g)) \sqrt{\frac{\nu_m}{ch}} \cos\left(\frac{m\pi}{c} x\right) \qquad (45e)$$

$$H_x^{IIIb_n} = j\sum_{m=0}^{\infty} \sqrt{Y_m^{III}}\ C_m^{IIIb_n} \sin(\beta_m^{III}(z+g)) \sqrt{\frac{\nu_m}{ch}} \cos\left(\frac{m\pi}{c} x\right) \qquad (45f)$$

where a_k^i and b_k^i are the amplitudes of the incident and reflected waves respectively in the region I (for i=I) and II (for i=II), β_k^i is the phase constant for mode k in the region i and is calculated with the equivalent dielectric constant of region III instead of ϵ_{eff} of region I or II. ν_k is the Neumann coefficient whose value is chosen equal to 1 for k=0 and 2 for k≠0. C_k^{III} is the wave amplitude of the field solutions in region III.

The magnetic fields of the region I and II can be matched to the magnetic field of region III separately because the structures that are superimposed (figure 18(b)) at

each reference plane have only one open boundary. The remaining reference planes of the substructures are closed by magnetic walls so that the magnetic field strengths vanish here. This was first suggested by Kuhn [9] in 1973. Applying Kuhn's method here leads finally to the following equations:

$$(a_N^I + b_N^I) = \sum_{P=0}^{\infty} \left[(a_P^I - b_P^I) A_1^{P,N} + \sum_{m=1}^{n} (a_P^{II_m} - b_P^{II_m}) B_{2,m}^{P,N} \right] \qquad (46a)$$

$$(a_N^{II_1} + b_N^{II_1}) = \sum_{P=0}^{\infty} \left[(a_P^I - b_P^I) B_{1,m}^{P,N} + \sum_{m=1}^{n} (a_P^{II_m} - b_P^{II_m}) A_2^{P,N} \right] \qquad (46b)$$

$$(a_N^{II_n} + b_N^{II_n}) = \sum_{P=0}^{\infty} \left[(a_P^I - b_P^I) B_{1,m}^{P,N} + \sum_{m=1}^{n} (a_P^{II_m} - b_P^{II_m}) A_2^{P,N} \right] \qquad (46c)$$

where

$$A_i^{P,N} = -j \sum_{K=0}^{\infty} \frac{Z_K^{III}}{\sqrt{Z_N^I Z_P^I}} K_i^{P,K} K_i^{N,K} \cot(\beta_K^{III} g) \qquad (47)$$

$$B_{1,m}^{P,N} = -j \sum_{K=0}^{\infty} \frac{Z_K^{III}}{\sqrt{Z_N^{II_m} Z_P^I}} \frac{K_1^{P,K} K_{2,m}^{N,K}}{\sin(\beta_K^{III} g)} \qquad (48)$$

$$B_{2,m}^{P,N} = -j \sum_{K=0}^{\infty} \frac{Z_K^{III}}{\sqrt{Z_N^I Z_P^{II_m}}} \frac{K_{2,m}^{P,K} K_1^{N,K}}{\sin(\beta_K^{III} g)} \qquad (49)$$

$$K_1^{N,K} = \frac{1}{h} \sqrt{\frac{\nu_K \nu_N}{ca}} \iint_{Z=-g} \cos\left(\frac{K\pi}{c} x\right) \cos\left(\frac{N\pi}{a} (x - -d_1)\right) dxdy \qquad (50a)$$

$$K_{2,m}^{P,M} = \frac{1}{h}\sqrt{\frac{\nu_M \nu_P}{cb}}\iint_{z=0}\cos\left(\frac{M\pi}{c}x\right)\cos\left(\frac{P\pi}{b}\left(x-d_2(m)\right)\right)dxdy \qquad (50b)$$

Results and Discussion :

This final equations system defined above for the calculation of the scattering parameters is an infinite linear set of equations and which has previously been solved numerically using only a finite number of series elements. The influence of the truncation on the calculated scattering parameters have been proved to gain an insight into the convergence behavior of the method as shown in figure 19. In this case, the ratio of the considered modes in different field regions has been kept equal to unity while the number of modes considered is varied. It can be seen that considering 8 or 10 modes is enough to get the results within acceptable accuracy. The larger the the number of modes considered, the more is time taken by the computer to simulate the results. Considering 8-10 modes is a good trade-off between accuracy and time, although here, as in all the other results shown, 10 modes have been considered.

Figure 20 shows the reflected power from port 1 (S_{11}) and transmitted powers in port 2 (S_{21}) and in port 3 (S_{31}) as well as the transmitted power from port 3 to port 2 (S_{23}) as a function of frequency for a 3db power divider. The dimensions of this microstrip

line power divider are taken such that input and output ports are the lines of characteristic impedance Z = 50 ohms (in this case width of the input and output lines are 73.1e-6 meters, height of the GaAs substrate as 1e-4 meters). It can be seen that the reflected power is less than 10% in the frequency range of 7-55GHz. Also, S_{23} is nearly zero for the entire frequency range. Some power is dissipated by the evanescent modes which are excited around 30GHz.

Figure 21 shows the effect of the width and length of the patch on the bandwidth of the divider. Here, again, the structure is a 3db power divider with input and output lines having characteristic impedances of 50 ohms (the width of the line = 73.1e-6 meters; the height of the substrate = 1e-4 meters; $\epsilon_r = 13.0$ for GaAs). It can be seen that the effect of reducing the width of the patch, while keeping the length of the patch constant, is to increase the bandwidth of the power divider (figure 21(b), plots for the value of "g = 1.5a"). Moreover, the length of the patch also plays an important role in defining the bandwidth.

Figure 22 ((a) for reflected power and (b) for transmitted power) shows the effect of the input line impedance on the performance of the divider when output line have characteristic impedance equal to 50ohms. It can be seen that as the characteristic impedance of the input line increases (i.e. the width of the input line decreases) the divider becomes more and more broadband with less reflected power at the input port. Figure 23 (again (a) for reflected power and (b) for transmitted power) shows

the effect of the position of the input line (in this case the characteristic impedance of the input line has been kept at 50ohms). The bandwidth of the structure is maximum when the input line is in the center, which finally leads to a 3db power divider.

Finally, figure 24 shows the performance of a power divider with the input line (port(1)) and the output lines (ports (2) and (3)) having characteristic impedances equal to 50 ohms. The divider is a 3db rectangular patch microstrip line structure with width of the patch (c) equal to three times the width of the input line and length of the patch (g) being 2.1 times the width of the input line. The divider has a bandwidth of more than 1 octave at the center frequency of 19GHz. (11.5GHz to 27GHz) with less than 10% reflected power in the frequency range of 12GHz till 16GHz and even less than 5% of the reflected power in the frequency range of 16GHz till 27GHz.

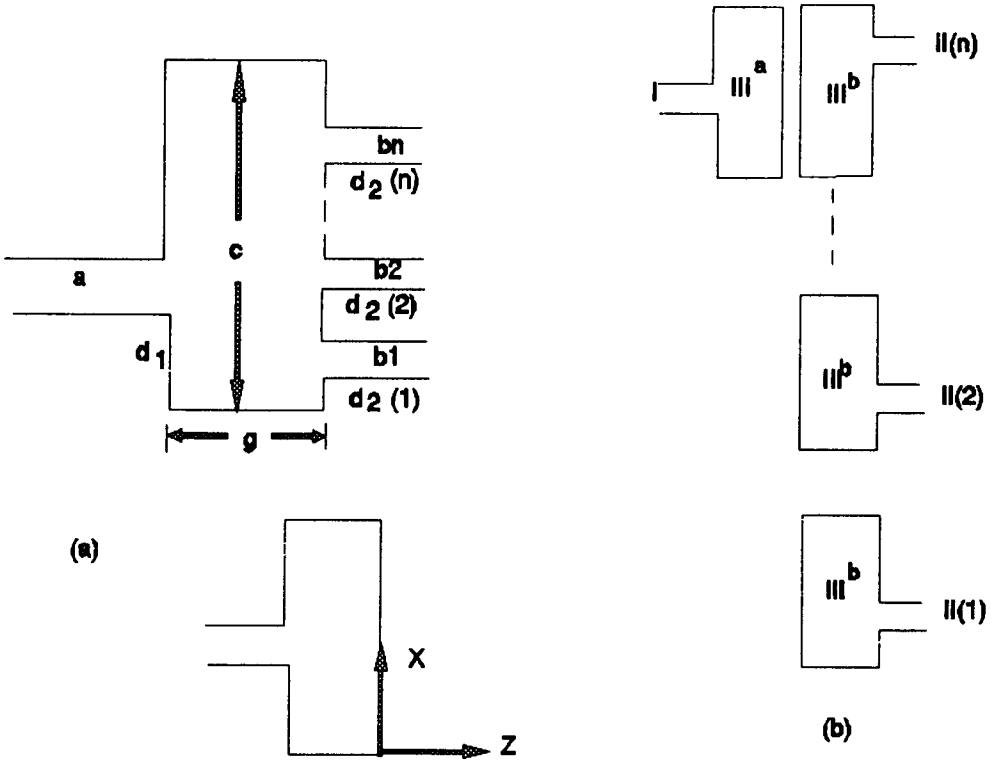

Figure 18 The interacting asymmetric double step with multiple output

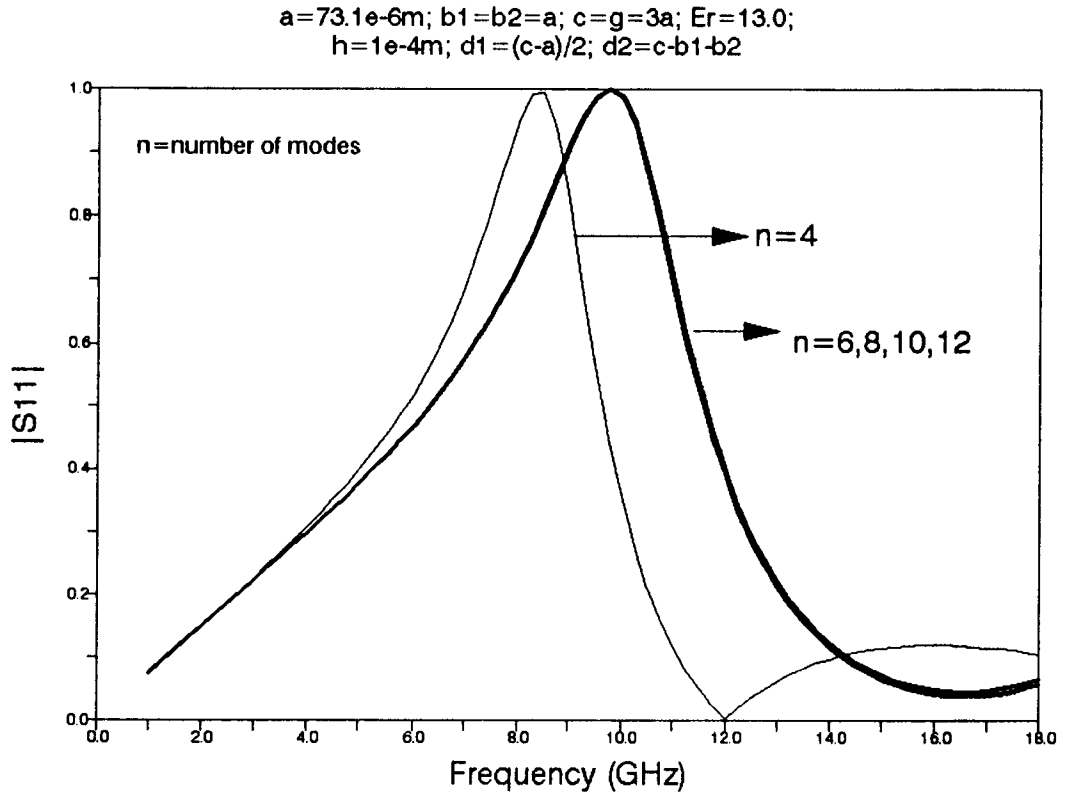

Figure 19 $|S_{11}|$ as a function of frequency for double step with two output lines with number of modes as a variable.

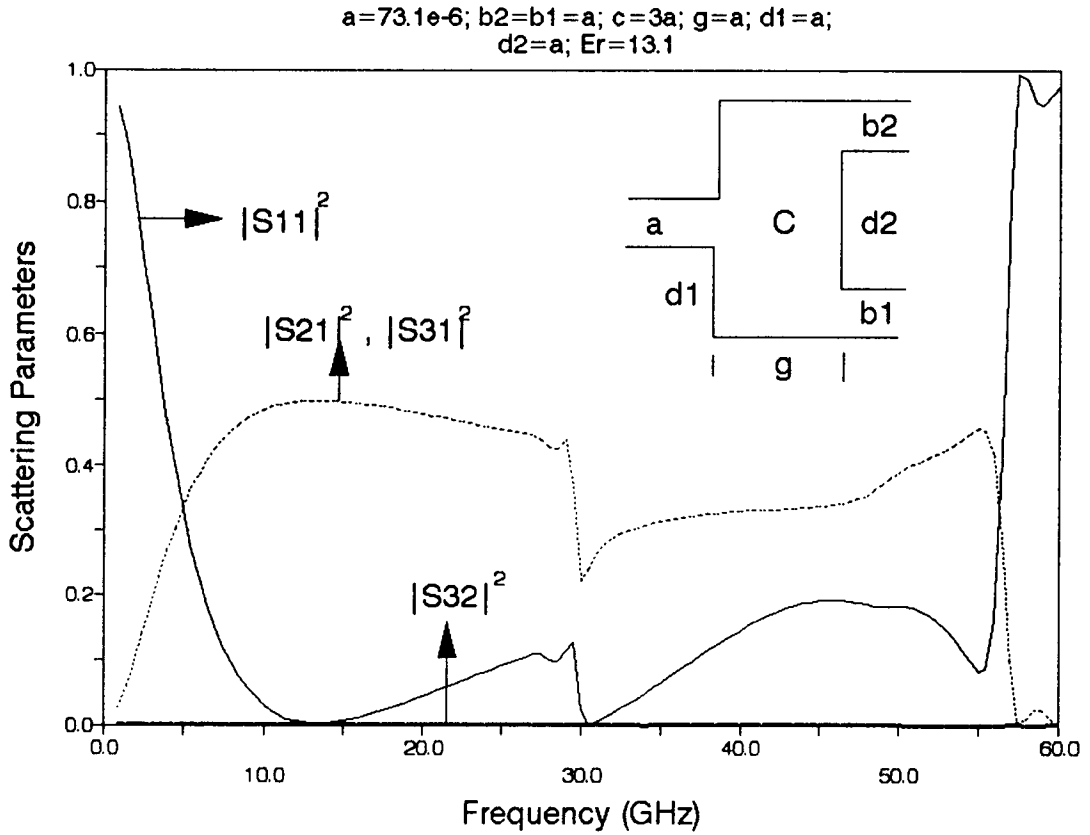

Figure 20 $|S_{ij}|^2$ as a function of frequency for a nominal 3db power divider.

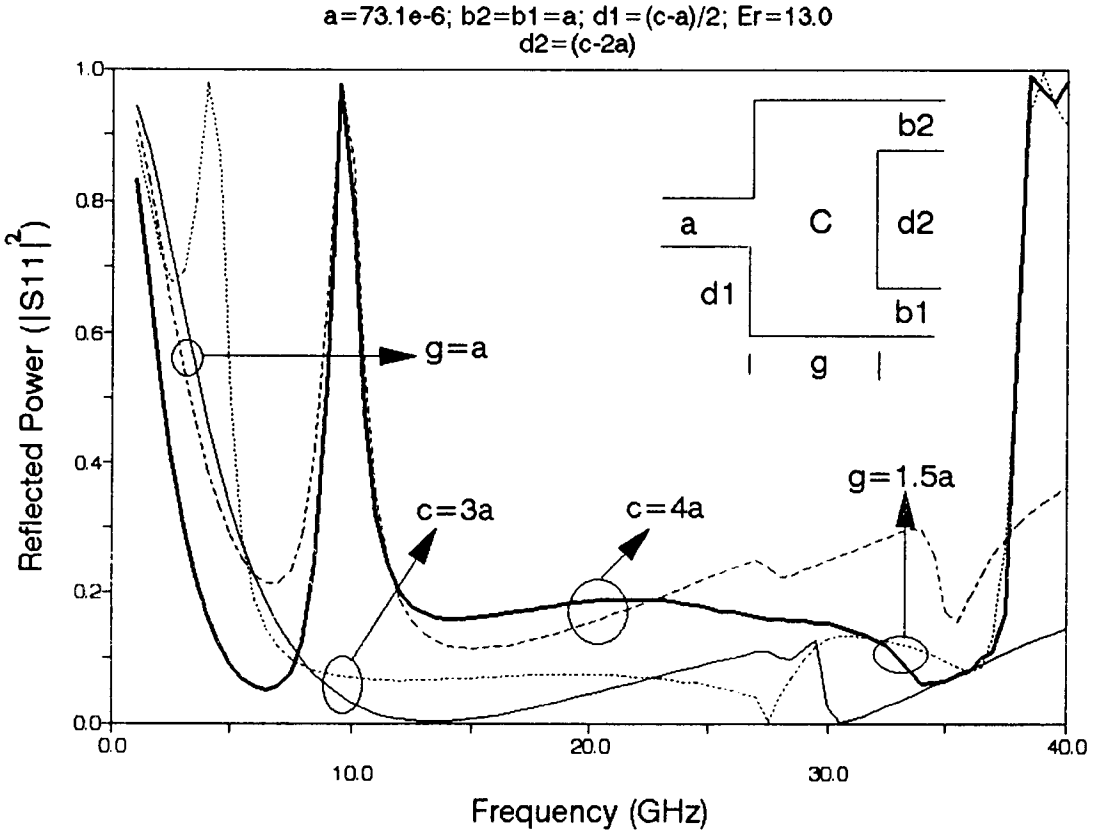

Figure 21a $|S_{11}|^2$ as a function of frequency for a 3db rectangular patch power divider with width and length of the patch as variables.

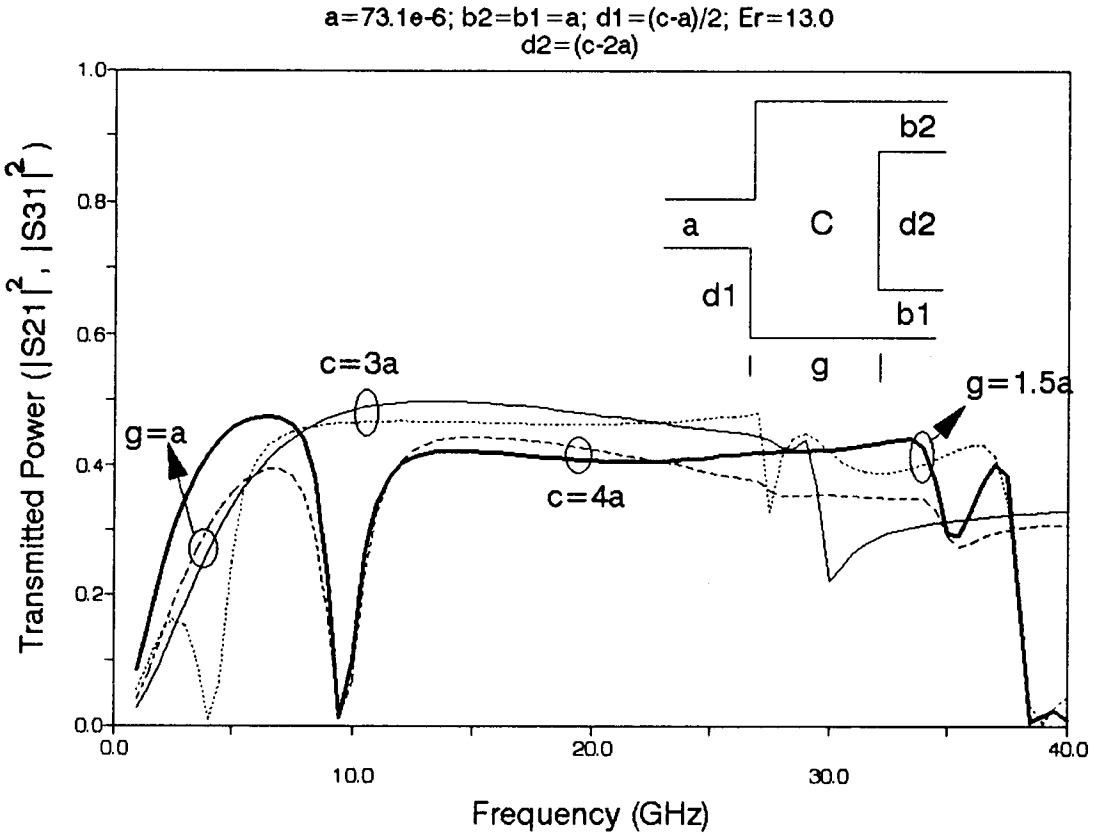

Figure 21b $|S_{21}|^2$ and $|S_{31}|^2$ as a function of frequency for a 3db rectangular patch power divider with width and length of patch as variables.

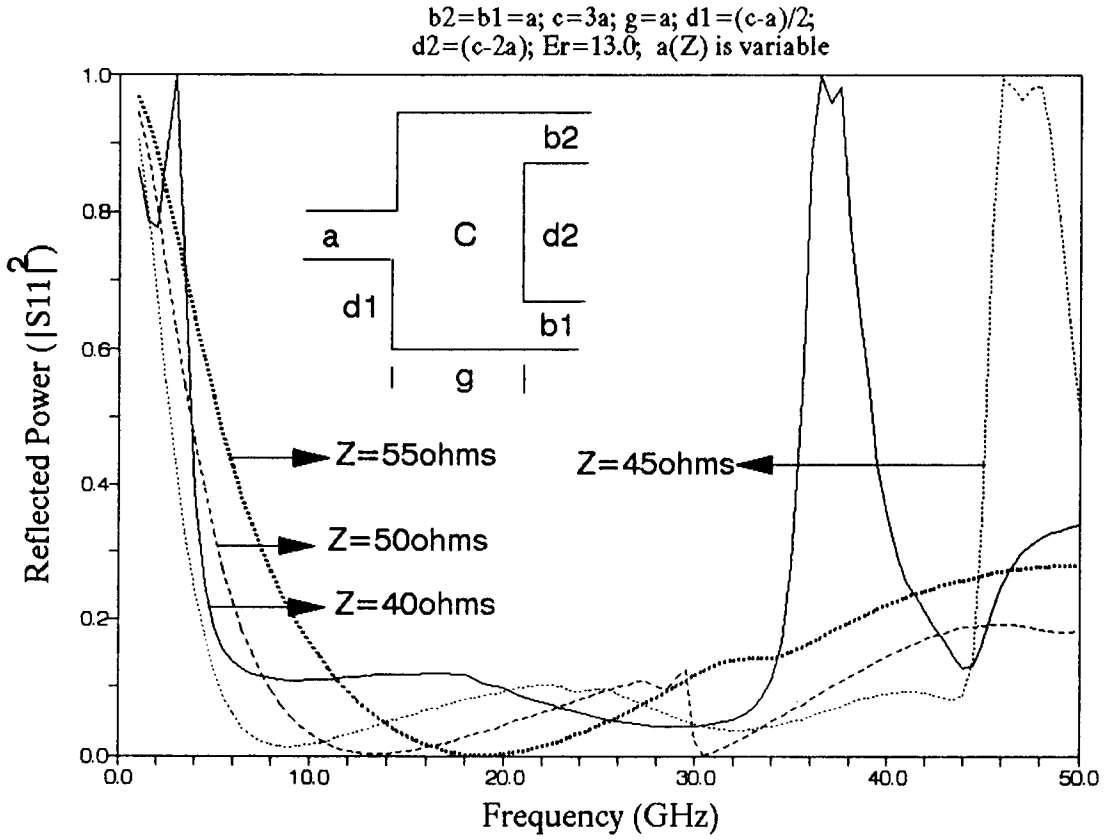

Figure 22a Effect of the impedance of input line on the reflected power as a function of frequency.

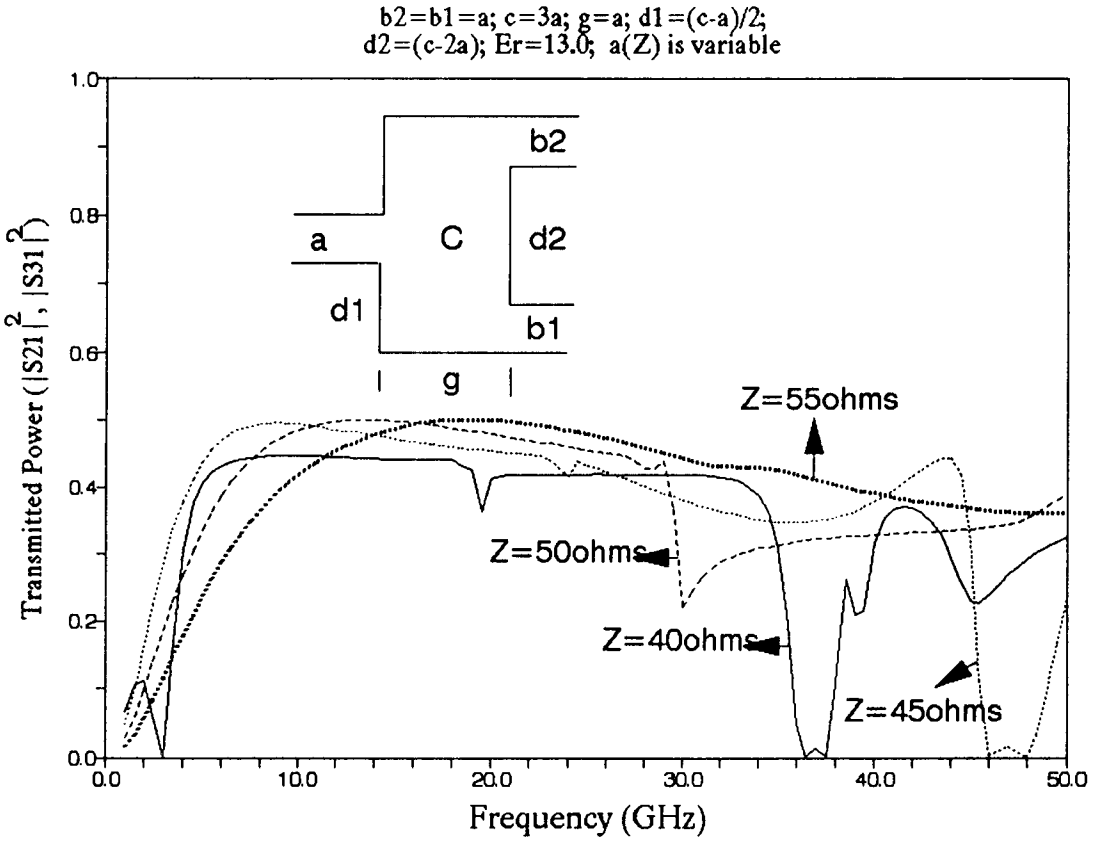

Figure 22b Effect of the impedance of input line on the transmitted power at ports 2 and 3 as a function of frequency.

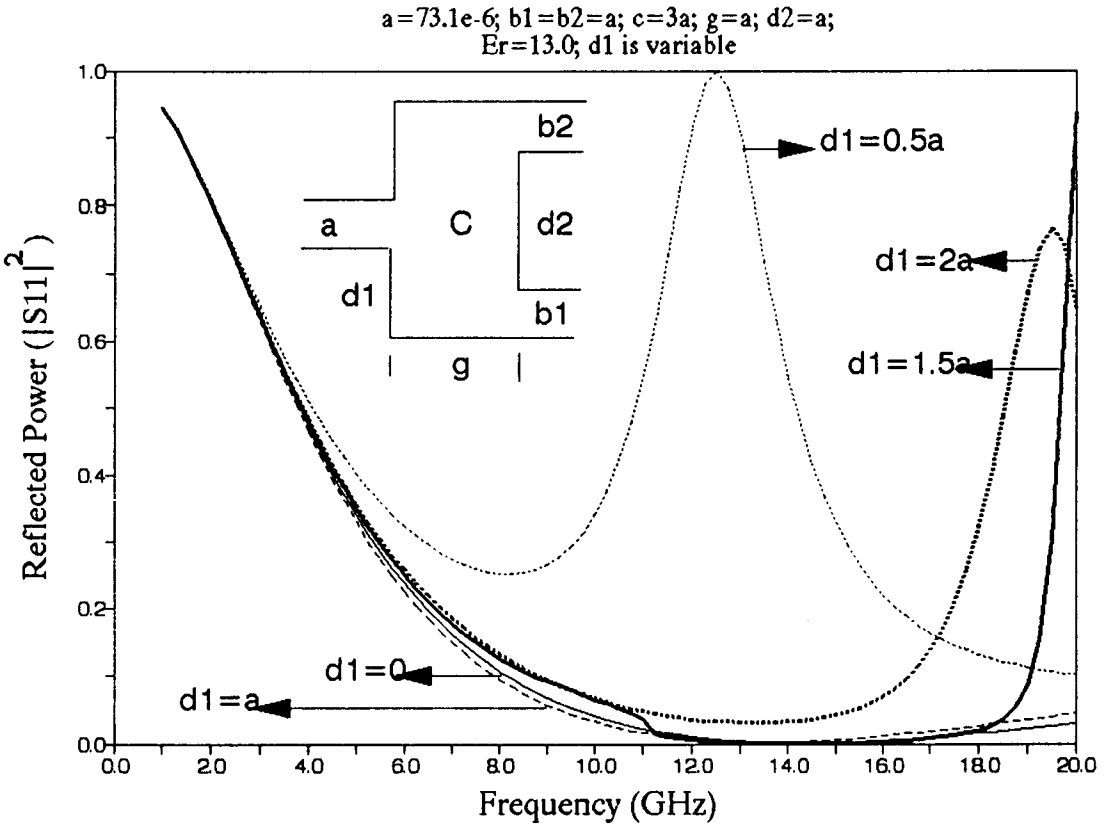

Figure 23a $|S_{11}|^2$ as a function of frequency with d_1 as a variable.

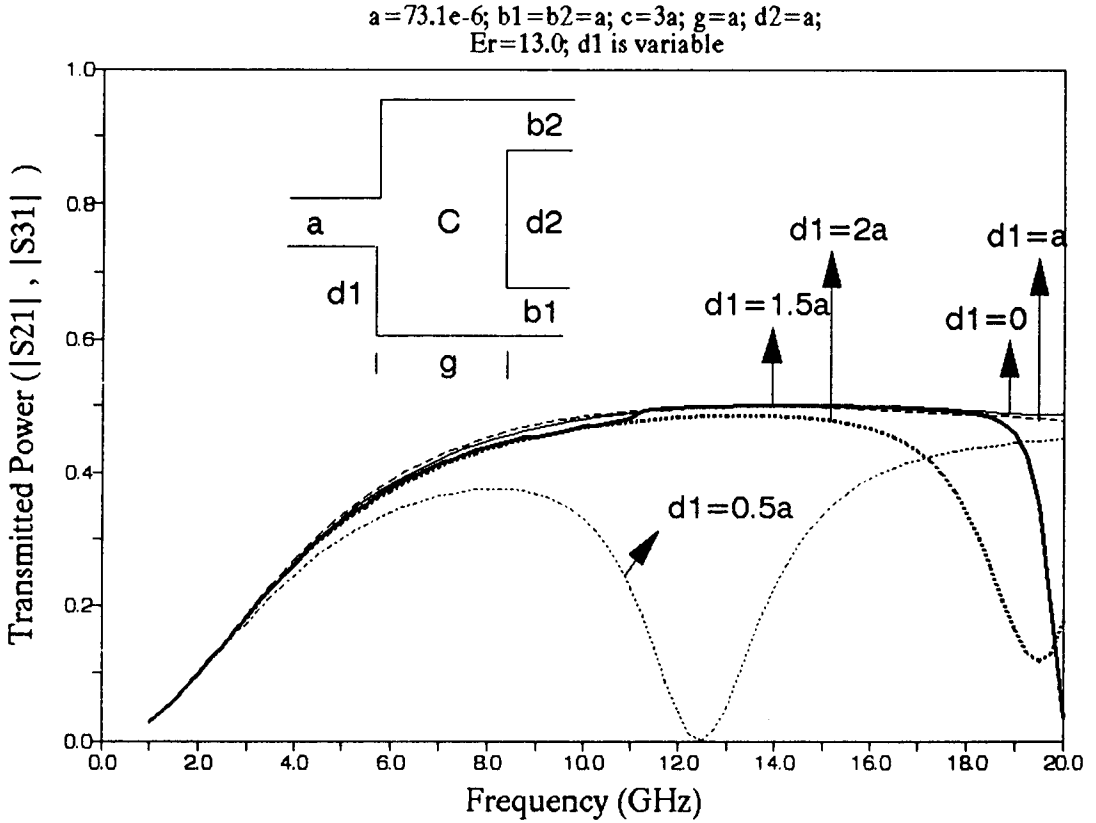

Figure 23b $|S_{21}|^2$ and $|S_{31}|^2$ as a function of frequency with d_1 as a variable.

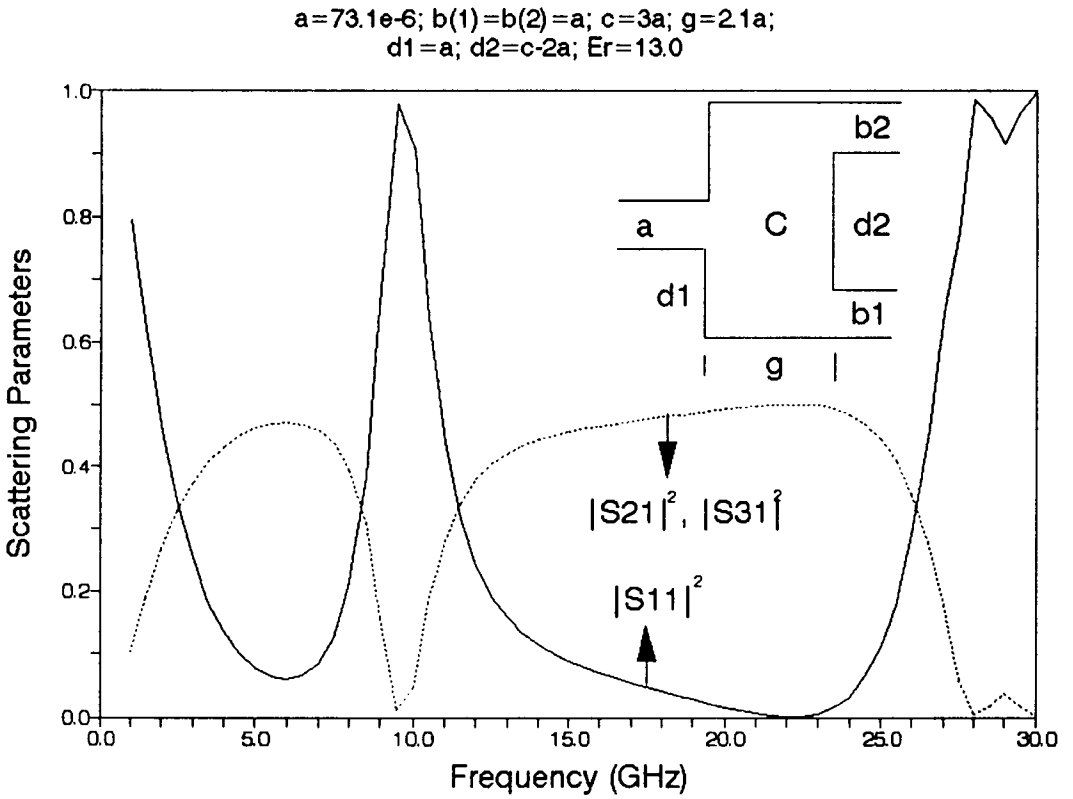

Figure 24 Scattering parameters as a function of frequency for a 3db rectangular patch power divider.

CONCLUSION

In this thesis, a numerical technique has been described to model microstrip discontinuities of various kinds. The method is based on a magnetic wall waveguide model that is assumed to be valid for describing the electromagnetic fields in the microstrip line and in the vicinity of microstrip line discontinuities. The mode matching method is used to describe the discontinuities after applying the waveguide model. The mode matching method is a general tool for the numerical computation of the electromagnetic field problems. It is a rigorous full-wave analysis suitable for the treatment of two or three dimensional field problems, including both scattering and eigen value problems. The straightforward formulation of this method makes it a very commonly used method among the personal computer users. However, compared to those methods that are problem oriented and optimized, the efficiency of this method is not very high. A characteristic advantage of the mode-matching technique is that it gives a better physical understanding of the effect of a junction or discontinuity in a guided wave structure. The disadvantage of this method being that it is limited to junctions whose discontinuity region belongs to a seperable coordinate system as compared to discretization methods, such as finite element and finite difference methods, which can be applied to junctions of arbitrary shapes. When combined with the generalized scattering matrix method, they together become a powerful tool for analyzing many practical composite waveguide structures. The generalized scattering method is useful for the analysis of complicated junction that

can be decomposed to several simpler junctions and also characterizing cascaded junctions that are in close proximity in terms of electrical length. The method is mathematically exact provided that all the matrices of infinite order are available. The results obtained using this technique are numerical models for microstripline discontinuities that are of medium numerical expense and of good accuracy and can be used in computer-aided circuit analysis even with a desktop computer.

The above explained technique is very useful in MICs and MMICs where (1) the problem of efficient matching of two microstrip lines with different characteristic impedances is to be tackled resulting in less reflection over a frequency band of interest; (2) the design of a filter for desired frequency band; (3) design of a power divider/combiner with desired bandwidth. The technique presented is compatible with the design of multiports with more than two outputs for applications as power combiners/dividers. In addition to experimental realization of the three ports discussed in this thesis, future work in this area should include computer-aided design of these multiports.

REFERENCES

1. M.Kirschning and R.H.Jansen, "Accurate model for effective dielectric constant of microstrip with validity up to millimeter-wave frequencies", Electronics Letters,vol.18,pp.272-273,1982.

2. R.H.Jansen, "Unified, user-oriented computation of shielded, covered and open planar microwave and millimeter-wave transmission-line characteristics", J.Microwaves, Opt. Acoust., vol.3,pp.14-22,1979.

3. H.Ermert, "Guiding and radiation characteristics of planar waveguides", IEE J. Microwaves, Opt. Acoust., vol.3,pp.59-62,March 1979.

4. H.A.Wheeler, "Transmission line properties of parallel wide strips by conformal mapping approximation", IEEE Trans. Microwave Theory Tech., vol.MTT-12,pp.280-289,1964.

5. H.A.Wheeler, "Transmission line properties of parallel strips seperated by a dielectric sheet", IEEE Trans. Microwave Theory Tech., vol.MTT-13,pp.172-185,1965.

6. G.Kompa, "S-matrix computation of microstrip discontinuities with a planar waveguide model", Arch. Elektron, Ubertragungstechn.,vol.30,pp.58-64, 1976.

7. I. Wolff and N.Knoppik, "Rectangular and circular microstrip disc capacitor and resonators", IEEE Trans.Microwave Theory and Technique, vol.MTT-22, pp.857-864,1974.

8. E.Kuhn, "A mode matching method for solving field problems in the waveguide and resonator circuits", Arch. Elektron Ubertragungstech., vol.27, pp.511-513, 1973.

9. Tatsuo Itoh, "Numerical techniques for microwave and millimeter-wave passive structures", John Wiley & Sons, New York.

10. Shih-Chang Wu, Hung-Yu Yang and Nicolaos G Alexopoulos,"A rigorous dispersive characterization of microstrip cross and tee junctions", 1990 IEEE MTT-S Digest, pp. 1151-1154.

11. P.B.Katehi and N.G.Alexopoulos,"Frequency dependent characteristics of microstrip discontinuities in millimeter wave integrated circuits", IEEE Trans. on Microwave Theory and Techniques, Vol. MTT-33, pp. 1029-1035, Oct.1985.

12. R.W.Jackson,"Full-wave finite element analysis of irregular microstrip discontinuities", IEEE Trans. on Microwave Theory and Techniques, Vol. MTT-37, pp. 81-89, Jan.1989.

13. J.R.Mosig,"Arbitrarily shaped microstrip structures and their analysis with a mixed potential integral equation", IEEE Trans. on Microwave Theory and Techniques, Vol. MTT-36, pp. 314-323, Feb.1988.

14. A.Khebir, A.B.Kouki and R.Mittra,"An efficient finite element approach for the analysis of three dimensional transmission line discontinuities using an asymptotic boundary condition", 1990 IEEE MTT-S Digest, pp. 1159-1162.

APPENDICES

APPENDIX 'A'

Putting equations 31-32 in 35 (pages 27-28) we finally get

$$\sqrt{Z_N^I}\ (a_N^I+b_N^I) = \sum_{K=0}^{\infty} \sqrt{Z_K^{III}}\ C_K^{IIIa} \cos(\beta_K^{III} g)\ K_3^{N,K} + \sum_{M=0}^{\infty} \sqrt{Z_M^{III}}\ C_M^{IIIb} K_4^{N,M}$$

where

$$K_3^{N,K} = \frac{1}{h}\sqrt{\frac{\nu_K \nu_N}{ca}} \int_{z=-g}\int \cos\left(\frac{K\pi}{c}x\right) \cos\left(\frac{N\pi}{a}(x-d_1)\right) dxdy$$

$$K_4^{N,M} = \frac{1}{h}\sqrt{\frac{\nu_M \nu_N}{ca}} \int_{z=-g}\int \cos\left(\frac{M\pi}{c}x\right) \cos\left(\frac{N\pi}{a}(x-d_1)\right) dxdy$$

Therefore

$$\sqrt{Z_N^I}\ (a_N^I+b_N^I) = \sum_{K=0}^{\infty} \sqrt{Z_K^{III}}\ C_K^{IIIa} \cos(\beta_K^{III} g)\ K_1^{N,K} + \sum_{M=0}^{\infty} \sqrt{Z_M^{III}}\ C_M^{IIIb} K_1^{N,M} \qquad (1)$$

$$\sqrt{Z_N^{II}}\ (a_N^{II}+b_N^{II}) = \sum_{M=0}^{\infty} \sqrt{Z_M^{III}}\ C_M^{IIIb} \cos(\beta_M^{III} g)\ K_2^{N,M} + \sum_{K=0}^{\infty} \sqrt{Z_K^{III}}\ C_K^{IIIa} K_2^{N,K} \qquad (2)$$

Now from equation(33)&(34) we get

$$C_K^{IIIa} = -j \sum_{N=0}^{\infty} \sqrt{\frac{Z_K^{III}}{Z_N^I}}\ (a_N^I - b_N^I)\ \frac{K_1^{N,K}}{\sin(\beta_K^{III} g)} \qquad (3)$$

$$C_M^{IIIb} = -j \sum_{P=0}^{\infty} \sqrt{\frac{Z_M^{III}}{Z_P^{II}}}\ (a_P^{II} - b_P^{II})\ \frac{K_2^{P,M}}{\sin(\beta_M^{III} g)} \qquad (4)$$

Therefore, equation(35) above becomes;

$$\sqrt{Z_N^I}\,(a_N^I+b_N^I)=\sum_{K=0}^{\infty}\sqrt{Z_K^{III}}\,[-j\sum_{P=0}^{\infty}\sqrt{\frac{Z_K^{III}}{Z_P^I}}\,(a_P^I-b_P^I)\,\frac{K_1^{P,K}}{\sin(\beta_K^{III}g)}]\cos(\beta_K^{III}g)\,K_1^{N,K}$$

$$+\sum_{M=0}^{\infty}\sqrt{Z_M^{III}}\,[-j\sum_{P=0}^{\infty}\sqrt{\frac{Z_M^{III}}{Z_P^{II}}}\,(a_P^{II}-b_P^{II})\,\frac{K_2^{P,M}}{\sin(\beta_M^{III}g)}]\,K_1^{N,M} \qquad (5)$$

Similarly, equation(36) can be written as;

$$\sqrt{Z_N^{II}}\,(a_N^{II}+b_N^{II})=\sum_{K=0}^{\infty}\sqrt{Z_K^{III}}\,[-j\sum_{P=0}^{\infty}\sqrt{\frac{Z_K^{III}}{Z_P^I}}\,(a_P^I-b_P^I)\,\frac{K_1^{P,K}}{\sin(\beta_K^{III}g)}]\,K_2^{N,K}$$

$$+\sum_{M=0}^{\infty}\sqrt{Z_M^{III}}\,[-j\sum_{P=0}^{\infty}\sqrt{\frac{Z_M^{III}}{Z_P^{II}}}\,(a_P^{II}-b_P^{II})\,\frac{K_2^{P,M}}{\sin(\beta_M^{III}g)}]\cos(\beta_M^{III}g)\,K_1^{N,M} \qquad (6)$$

These equations(38) can be written as (after some mathematics);

$$(a_N^I + b_N^I) = \sum_{P=0}^{\infty}[\,(a_P^I - b_P^I)\,A_1^{P,N} + (a_P^{II} - b_P^{II})\,B_2^{P,N}] \qquad (7)$$

$$(a_N^{II} + b_N^{II}) = \sum_{P=0}^{\infty}[\,(a_P^I - b_P^I)\,B_1^{P,N} + (a_P^{II} - b_P^{II})\,A_2^{P,N}] \qquad (8)$$

where

$$A_i^{P,N} = -j\sum_{K=0}^{\infty}\frac{Z_K^{III}}{\sqrt{Z_N^i Z_P^I}}\,K_i^{P,K}K_i^{N,K}\cot(\beta_K^{III}g) \qquad (9)$$

$$B_i^{P,N} = -j\sum_{K=0}^{\infty}\frac{Z_K^{III}}{\sqrt{Z_N^{i'} Z_P^i}}\,\frac{K_i^{P,K}K_{i'}^{N,K}}{\sin(\beta_K^{III}g)} \qquad (10)$$

(i=1 or 2 and i'=1 for i=2 & i'=2 for i=1)

APPENDIX 'B'

Equations 44-45 (page 46-47) can be written as :

$$E_y^I = \sum_{K=0}^{\infty} \sqrt{Z_K^I}\ (a_K^I e^{-j\beta_K^I(z+g)} + b_K^I e^{j\beta_K^I(z+g)}) \sqrt{\frac{\nu_K}{ah}} \cos\left(\frac{k\pi}{a}(x-d_1)\right) \qquad (1a)$$

$$H_x^I = -\sum_{K=0}^{\infty} \sqrt{Y_K^I}\ (a_K^I e^{-j\beta_K^I(z+g)} - b_K^I e^{j\beta_K^I(z+g)}) \sqrt{\frac{\nu_K}{ah}} \cos\left(\frac{k\pi}{a}(x-d_1)\right) \qquad (1b)$$

$$E_y^{II_1} = \sum_{m=0}^{\infty} \sqrt{Z_m^{II_1}}\ (a_m^{II_1} e^{j\beta_m^{II_1} z} + b_m^{II_1} e^{-j\beta_m^{II_1} z}) \sqrt{\frac{\nu_m}{b_1 h}} \cos\left(\frac{m\pi}{b_1}(x-d_2)\right) \qquad (1c)$$

$$H_x^{II_1} = \sum_{m=0}^{\infty} \sqrt{Y_m^{II_1}}\ (a_m^{II_1} e^{j\beta_m^{II_1} z} - b_m^{II_1} e^{-j\beta_m^{II_1} z}) \sqrt{\frac{\nu_m}{b_1 h}} \cos\left(\frac{m\pi}{b_1}(x-d_2)\right) \qquad (1d)$$

$$\vdots$$

$$E_y^{II_n} = \sum_{m=0}^{\infty} \sqrt{Z_m^{II_n}}\ (a_m^{II_n} e^{j\beta_m^{II_n} z} + b_m^{II_n} e^{-j\beta_m^{II_n} z}) \sqrt{\frac{\nu_m}{b_n h}} \cos\left(\frac{m\pi}{b_n}(x-d_2(n))\right) \qquad (1e)$$

$$H_x^{II_n} = \sum_{m=0}^{\infty} \sqrt{Y_m^{II_n}}\ (a_m^{II_n} e^{j\beta_m^{II_n} z} - b_m^{II_n} e^{-j\beta_m^{II_n} z}) \sqrt{\frac{\nu_m}{b_n h}} \cos\left(\frac{m\pi}{b_n}(x-d_2(n))\right) \qquad (1f)$$

$$E_y^{IIIa} = \sum_{K=0}^{\infty} \sqrt{Z_K^{III}}\ C_K^{IIIa} \cos(\beta_K^{III} z) \sqrt{\frac{\nu_K}{ch}} \cos\left(\frac{K\pi}{c}x\right) \qquad (2a)$$

$$H_x^{IIIa} = j\sum_{K=0}^{\infty} \sqrt{Y_K^{III}}\ C_K^{IIIa} \sin(\beta_K^{III} z) \sqrt{\frac{\nu_K}{ch}} \cos\left(\frac{K\pi}{c}x\right) \qquad (2b)$$

$$E_y^{IIIb_1} = \sum_{m=0}^{\infty} \sqrt{Z_m^{III}}\ C_m^{IIIb_1} \cos(\beta_m^{III}(z+g)) \sqrt{\frac{\nu_m}{ch}} \cos\left(\frac{m\pi}{c}x\right) \qquad (2c)$$

$$H_x^{IIIb_1} = j\sum_{m=0}^{\infty} \sqrt{Y_m^{III}}\ C_m^{IIIb_1} \sin(\beta_m^{III}(z+g)) \sqrt{\frac{\nu_m}{ch}} \cos(\frac{m\pi}{c}x) \qquad (2d)$$

$$E_y^{IIIb_n} = \sum_{m=0}^{\infty} \sqrt{Z_m^{III}}\ C_m^{IIIb_n} \cos(\beta_m^{III}(z+g)) \sqrt{\frac{\nu_m}{ch}} \cos(\frac{m\pi}{c}x) \qquad (2e)$$

$$H_x^{IIIb_n} = j\sum_{m=0}^{\infty} \sqrt{Y_m^{III}}\ C_m^{IIIb_n} \sin(\beta_m^{III}(z+g)) \sqrt{\frac{\nu_m}{ch}} \cos(\frac{m\pi}{c}x) \qquad (2f)$$

Now applying the normal mode-matching technique as was suggested by Kuhn's [8], at the interface of I and III[a], equations can be written as:

$$j\sqrt{Y_K^{III}}\ C_K^{IIIa} \sin(\beta_K^{III} g) = \sum_{N=0}^{\infty} \sqrt{Y_N^{I}}\,(a_N^I - b_N^I)\ K_1^{N,K} \qquad (3a)$$

where

$$K_1^{N,K} = \frac{1}{h}\sqrt{\frac{\nu_K \nu_N}{ca}} \int_{z=-g}\int \cos(\frac{K\pi}{c}x) \cos(\frac{N\pi}{a}(x-d_1))\, dxdy \qquad (3b)$$

and is known as coupling integral.

Similarly, at the interface of region II and III, the result is:

$$j\sqrt{Y_{M1}^{III}}\ C_{M1}^{IIIb_1} \sin(\beta_{M1}^{III} g) = \sum_{P1=0}^{\infty} \sqrt{Y_{P1}^{II_{b_1}}}\,(a_{P1}^{II_{b_1}} - b_P^{II_{b_1}})\ K_{2,1}^{P1,M1} \qquad (4a)$$

$$j\sqrt{Y_{Mn}^{III}}\ C_{Mn}^{IIIb_n} \sin(\beta_{Mn}^{III} g) = \sum_{Pn=0}^{\infty} \sqrt{Y_{Pn}^{II_{b_n}}}\,(a_{Pn}^{II_{b_n}} - b_{pn}^{II_{b_n}})\ K_{2,n}^{Pn,Mn} \qquad (4b)$$

where

$$K_{2,m}^{P,M} = \frac{1}{h}\sqrt{\frac{\nu_M \nu_P}{c b_m}}\int_{z=0}\int \cos\left(\frac{M\pi}{c}x\right)\cos\left(\frac{P\pi}{b_m}\left(x-d_2(m)\right)\right)dxdy \qquad (4c)$$

Now the magnetic fields of the subregions are matched. If the total electromagnetic field is calculated, the field solutions (1-2), taking into account equations (3) and (4) and the electric field strengths of waveguides I and II and the total electric field in the connecting field region III are additionally matched at the reference planes. So the boundary conditions at the boundary between region I and III that must be fulfilled by the fields is

$$E_{\tan}^{I}\big|_{z=-g} = E_{\tan}^{IIIa}\big|_{z=-g} + E_{\tan}^{IIIb_1}\big|_{z=-g} + \ldots + E_{\tan}^{IIIb_N}\big|_{z=-g} \qquad (5)$$

Similarly, applying the boundary condition between regions II and III gives

$$E_{\tan}^{II}\big|_{z=0} = E_{\tan}^{IIIa}\big|_{z=0} + E_{\tan}^{IIIb_1}\big|_{z=0} + \ldots + E_{\tan}^{IIIb_n}\big|_{z=0} \qquad (6)$$

Using equations 1-4 and doing some mathematics, we get;

$$\sqrt{Z_N^I}\left(a_N^I + b_N^I\right) = \sum_{K=0}^{\infty}\sqrt{Z_K^{III}}\,C_K^{IIIa}\cos\left(\beta_K^{III}g\right)K_1^{N,K} + \sum_{M1=0}^{\infty}\sqrt{Z_{M1}^{III}}\,C_{M1}^{IIIb_1}K_1^{N,M1}$$

$$+ \sum_{M2=0}^{\infty}\sqrt{Z_{M2}^{III}}\,C_{M2}^{IIIb_2}K_1^{N,M2} + \ldots + \sum_{Mn=0}^{\infty}\sqrt{Z_{Mn}^{III}}\,C_{Mn}^{IIIb_n}K_1^{N,Mn} \qquad (7)$$

$$\sqrt{Z_N^{IIb_1}}\left(a_N^{IIb_1} + b_N^{IIb_1}\right) = \sum_{M1=0}^{\infty}\sqrt{Z_{M1}^{III}}\,C_{M1}^{IIIb_1}\cos\left(\beta_{M1}^{III}g\right)K_{2,1}^{N,M1} + \sum_{K=0}^{\infty}\sqrt{Z_K^{III}}\,C_K^{IIIa}K_{2,1}^{N,K}$$

$$+ \sum_{M2=0}^{\infty}\sqrt{Z_{M2}^{III}}\,C_{M2}^{IIIb_2}\cos\left(B_{M2}^{III}g\right)K_{2,2}^{N,M2} + \ldots + \sum_{Mn=0}^{\infty}\sqrt{Z_{Mn}^{III}}\,C_{Mn}^{IIIb_n}\cos\left(B_{M2}^{III}g\right)K_1^{N,M}$$

....(8)

$$\sqrt{Z_N^{IIb_n}}\,(a_N^{IIb_n}+b_N^{IIb_n}) = \sum_{M1=0}^{\infty}\sqrt{Z_{M1}^{III}}\,C_{M1}^{IIIb_1}\cos(\beta_{M1}^{III}g)\,K_{2,1}^{N,M1}+\sum_{K=0}^{\infty}\sqrt{Z_K^{III}}\,C_K^{IIIa}K_{2,1}^{N,K}$$

$$+\sum_{M2=0}^{\infty}\sqrt{Z_{M2}^{III}}\,C_{M2}^{IIIb_2}Cos(B_{M2}^{III}g)\,K_{2,2}^{N,M2}+\;..\;+\sum_{Mn=0}^{\infty}\sqrt{Z_{Mn}^{III}}\,C_{Mn}^{IIIb_n}COS(B_{M2}^{III}g)\,K_1^{N,M}$$

....(9)

Now from equation(3)&(4) we get

$$C_K^{IIIa} = -j\sum_{N=0}^{\infty}\sqrt{\frac{Z_K^{III}}{Z_N^{I}}}\,(a_N^{I}-b_N^{I})\,\frac{K_1^{N,K}}{\sin(\beta_K^{III}g)} \qquad (9)$$

$$C_M^{IIIb_i} = -j\sum_{P=0}^{\infty}\sqrt{\frac{Z_M^{III}}{Z_P^{IIb_i}}}\,(a_P^{IIb_i}-b_P^{IIb_i})\,\frac{K_{2,i}^{P,M}}{\sin(\beta_M^{III}g)} \qquad (10)$$

where i stands for the ith output line.

Therefore, equation 7-9, above, becomes;

$$\sqrt{Z_N^{I}}\,(a_N^{I}+b_N^{I}) = \sum_{K=0}^{\infty}\sqrt{Z_K^{III}}\,[-j\sum_{P=0}^{\infty}\sqrt{\frac{Z_K^{III}}{Z_P^{I}}}\,(a_P^{I}-b_P^{I})\,\frac{K_1^{P,K}}{\sin(\beta_K^{III}g)}]\cos(\beta_K^{III}g)\,K_1^{N,K}$$

$$+\sum_{M=0}^{\infty}\sqrt{Z_M^{III}}\,[-j\sum_{P=0}^{\infty}\sqrt{\frac{Z_M^{III}}{Z_P^{II}}}\,(a_P^{II}-b_P^{II})\,\frac{K_2^{P,M}}{\sin(\beta_M^{III}g)}]\,K_1^{N,M} \qquad (5)$$

Similarly, equation(36) can be written as;

$$\sqrt{Z_N^{II}}\,(a_N^{II}+b_N^{II}) = \sum_{K=0}^{\infty}\sqrt{Z_K^{III}}\,[-j\sum_{P=0}^{\infty}\sqrt{\frac{Z_K^{III}}{Z_P^{I}}}\,(a_P^{I}-b_P^{I})\,\frac{K_1^{P,K}}{\sin(\beta_K^{III}g)}]\,K_2^{N,K}$$

$$+\sum_{M=0}^{\infty}\sqrt{Z_M^{III}}\,[-j\sum_{P=0}^{\infty}\sqrt{\frac{Z_M^{III}}{Z_P^{II}}}\,(a_P^{II}-b_P^{II})\,\frac{K_2^{P,M}}{\sin(\beta_M^{III}g)}]\cos(\beta_M^{III}g)\,K_1^{N,M} \qquad (6)$$

APPENDIX C

```
c       This program had been written by Sunil Kapoor on 02/04/92 as a part
c       of his MSEE thesis at Oregon State University, Corvallis.
c
c       This program calculates the Scattering parameters of the Interacting
c       assymetric double step microstrip discontinuities.
c
c       'N' in the PARAMETER statement (Nn in the 'AINV' subroutine)
c       represents the dimension for the number of modes to be considered.

        PARAMETER (N=50,M=N*2)
        COMMON/CONST/PI,AMU0,EPS0,EPSEFF(6),OMEGA,WEFF(6),NUM
        COMMON/DIM/ A,B,C,D,D1,D2,H,ER,G,tt
        COMMON/FUNC/ FUNK(2,N,N),beta(N,3)
        COMPLEX AFUN,BFUN,CFUN,DFUN,S(M,1),BETA(N,3),Z,X1(M,M),
     1  X2(M,1),FUN1,X1INV(M,M),betag,S11,S12,S21,S22
        integer iqn
        OPEN (UNIT=11,NAME="output")

c       A is the width of input line
c       B is the width of output line
c       C is the width of middle line
c       D1 is the distance from bottom of C till A starts
c       D2 is the distance from bottom of C till B starts
C       G is the length of middle line
c       H is the height of the substrate
c       NUM is the no. of modes to be considered

        write(*,*)'Write the values of width of the input line (meters)'
        read (*,*) a
        write(*,*)'Write the value of width of the output line in terms of the'
        write(*,*)'input line (b/a)'
        read(*,*) br
        write(*,*)'Write the value of width of the middle line in terms of the'
        write(*,*)'input line (c/a)'
        read(*,*) cr
        write(*,*)'Write the value of length of the middle line in terms of the'
        write(*,*)'input line (g/a)'
        read(*,*) gr
        write(*,*)'Write the value of the offset of the input line from the'
        write(*,*)'bottom of the middle line, in terms of a (d1/a)'
        read(*,*) d1r
```

```
      write(*,*)'Write the value of the offset of the output line from the'
      write(*,*)'bottom of the middle line, in terms of a (d2/a)'
      read(*,*) d2r
      write(*,*)'Write the value of the Dielectric Constant Erof substrate'
      read (*,*) er
      write(*,*)'Write the value of height of the substrate'
      read (*,*) h
      write(*,*)'write the freq in GHz ;  min, max, inc'
      read(*,*)fmin,fmax,fincr
      write(*,*)'write the no. of modes to be considered'
      read(*,*)num

      b=a*br
      c=a*cr
      d1=a*d1r
      d2=a*d2r
      g=a*gr

      write(11,*)'a,b,c',a,b,c
      write(11,*)'d1,d2,g',d1,d2,g
      write(11,*)'er,h',er,h
      write(11,*)'num',num
      WRITE(11,*)'freq,S11MAG,S21MAG,sum'

      TT=.0
      PI=3.14159265358979
      AMU0=1.26E-6
      EPS0=8.854185E-12
      h=h*1000.0
 2    FREQ=fMIN
 3    OMEGA=2.0*PI*FREQ*1.0e9

c     Following DO LOOP calculates the equivalent widths of the strips
c     using waveguide model (subroutine EPSL)

      DO 5 IREG=1,3
      IF(IREG.EQ.1) W=A
      IF(IREG.EQ.2) W=B
      IF(IREG.EQ.3) W=C
      w=w*1000.0
      CALL EPSL(FREQ,W,EEFFF,WEFFF,XIFFF)
      EPSEFF(IREG)=EEFFF
      WEFF(IREG)=WEFFF/1000.0
 5    continue
```

```
      dc=abs(c-weff(3))/2
      da=abs(a-weff(1))/2
      db=abs(b-weff(2))/2
      weff(4)=d1+dc-da
      weff(5)=d2+dc-db
      weff(6)=g
      if (d1.eq.0.) weff(4)=0.
      if (d2.eq.0.) weff(5)=0.
      h=h/1000.0

c     'funka' is function 'A' resulting after using Mode-matching technique

      do 9 ksa=0,num-1
      do 8 is=1,2
      do 7 msa=0,num-1
      call funka(is,msa,ksa)
 7    continue
      call beeta(ksa,is)
 8    continue
      call beeta(ksa,3)
 9    continue

      DO 20 KKS=1,NUM
      KS=KKS-1
      DO 10 MMS=1,NUM
      MS=MMS-1
c
c     X1 is the matrix which is associated with reflection coefficients
c
      X1(KKS,MMS)=CFUN(1,MS,KS)
      X1(NUM+KKS,MMS)=BFUN(1,MS,KS)
      X1(KKS,NUM+MMS)=BFUN(2,MS,KS)
      X1(NUM+KKS,NUM+MMS)=CFUN(2,MS,KS)
 10   CONTINUE
c
c     X2 is the matrix which is associated with incident coefficients
c
      X2(KKS,1)=X1(KKS,1)
      if (kks.eq.1) x2(kks,1)=x2(kks,1)-cmplx(2.0,0.0)
      X2(NUM+KKS,1)=X1(NUM+KKS,1)
 20   CONTINUE
c
c     NUM2 defines the dimension of X1 matrix
c
```

```
      NUM2=NUM*2
C     Calculating the inverse of matrix X1 and storing as X1INV
      CALL AINV(X1,NUM2,X1INV)
C     Calculating the product of matrices X1INV and X2 and storing as S
      CALL PRODUCT(X1INV,X2,NUM2,S)
      S11=S(1,1)
      S21=S(NUM+1,1)
      S11MAG=CABS(S11)
      S21MAG=CABS(S21)
      sum=s11mag**2.0 + s21mag**2.0
      WRITE(11,199)freq,S11MAG,S21MAG,sum
 199  format(1x,f6.3,5x,e15.7,5x,e15.7,5x,e15.7)
      WRITE(*,*)freq,S11MAG,S21MAG,sum
      FREQ=FREQ+fincr
      if(freq.le.fmax) go to 3
      if(iqn.eq.1) go to 300
 200  CONTINUE
 300  continue
      STOP
      END

      SUBROUTINE BEETA(NM,IREG)
      PARAMETER (N=50,M=N*2)
      COMMON/CONST/PI,AMU0,EPS0,EPSEFF(6),OMEGA,WEFF(6),NUM
      COMMON/FUNC/ FUNK(2,N,N),beta(N,3)
      COMPLEX BETA(N,3)
      AK0SQ=AMU0*EPS0*EPSEFF(IREG)*OMEGA*OMEGA
      AK1SQ=(NM*PI/WEFF(IREG))**2.0
      IF(AK0SQ.GE.AK1SQ)
      BETA(nm+1,ireg)=cmplx(SQRT(AK0SQ-AK1SQ),0.)
      IF(AK0SQ.LT.AK1SQ) BETA(nm+1,ireg)=cmplx(0.,SQRT(AK1SQ-AK0SQ))
      END

      SUBROUTINE FUNKA(ISUB,MSA,KCA)
      PARAMETER (N=50,M=N*2)
      COMMON/CONST/PI,AMU0,EPS0,EPSEFF(6),OMEGA,WEFF(6),NUM
      COMMON/FUNC/ FUNK(2,N,N),beta(N,3)
c
c     AB is the width of the line of region ISUB
c     D is the distance from z-axis till the ISUB region's line starts
c     C is the width of the middle region (i.e.3rd)
c
      nu=1
      if(msa.ne.0.or.kca.ne.0) nu=2
```

```
      if(msa.ne.0.AND.kca.ne.0) nu=4
      AB=WEFF(ISUB)
      D=WEFF(ISUB+3)
      C=WEFF(3)
      X1=SQRT(NU/(AB*C))
      X2=PI*KCA/C
      X3=PI*MSA/AB
      if (msa.eq.0 .and. kca.eq.0) go to 10
      go to 20
10    funk(isub,1,1)=x1*ab
      go to 50
20    if (x2.eq.x3) go to 30
      go to 40
30    funk(isub,msa+1,kca+1)=x1*cos(x2*d)*ab/2.0
      go to 50
40    funk(isub,msa+1,kca+1)=x1*x2*sin(x2*d)/(x3**2 - x2**2)
50    return
      end


      FUNCTION CFUN(ISUB,MS,KS)
      PARAMETER (N=50,M=N*2)
      COMMON/CONST/PI,AMU0,EPS0,EPSEFF(6),OMEGA,WEFF(6),NUM
      COMMON/FUNC/ FUNK(2,N,N),beta(N,3)
      COMPLEX AFUN,BFUN,CFUN,BETA(N,3),FUN1,BETAG
      AFUN=CMPLX(0.,0.)
      DO 10 KC=0,NUM-1
      BETAG=BETA(KC+1,3)*cmplx(WEFF(6),0.)
      FUN1=cmplx(FUNK(ISUB,MS+1,KC+1)*FUNK(ISUB,KS+1,KC+1),0.)
      FUN1=FUN1*CSQRT(BETA(MS+1,ISUB)*BETA(KS+1,ISUB))/
     1                                  BETA(KC+1,3)
      FUN1=FUN1*CCOS(BETAG)/CSIN(BETAG)
      AFUN=AFUN+FUN1
10    CONTINUE
      AFUN=CMPLX(0.,-1.)*AFUN
      cfun=afun
      if(ms.eq.ks) cfun=cfun+cmplx(1.0,0.0)
      RETURN
      END

      FUNCTION BFUN(ISUB,MS,KS)
      PARAMETER (N=50,M=N*2)
      COMMON/CONST/PI,AMU0,EPS0,EPSEFF(6),OMEGA,WEFF(6),NUM
      COMMON/FUNC/ FUNK(2,N,N),beta(N,3)
```

```
      COMPLEX BFUN,BETA(N,3),FUN1,BETAG
      IF(ISUB.EQ.1) ISUBN=2
      IF(ISUB.EQ.2) ISUBN=1
      BFUN=CMPLX(0.,0.)
      DO 10 KC=0,NUM-1
      BETAG=BETA(KC+1,3)*cmplx(WEFF(6),0.)
      FUN1=cmplx(FUNK(ISUB,MS+1,KC+1)*FUNK(ISUBN,KS+1,KC+1),0.)
      FUN1=FUN1*CSQRT(BETA(MS+1,ISUB)*BETA(KS+1,ISUBN))/
     1                                BETA(KC+1,3)
      FUN1=FUN1/CSIN(BETAG)
      BFUN=BFUN+FUN1
   10 CONTINUE
      BFUN=CMPLX(0.,-1.)*BFUN
      END


      SUBROUTINE PRODUCT(X,Y,Nn,Z)
      PARAMETER(N=50,M=N*2)
      COMPLEX X(M,M),Y(M,1),Z(M,1)
      DO 10 I=1,Nn
      Z(I,1)=CMPLX(0.,0.)
      DO 10 J=1,Nn
      Z(I,1)=Z(I,1)+(X(I,J)*Y(J,1))
   10 CONTINUE
      RETURN
      END

      SUBROUTINE AINV(X,N,TM)
      PARAMETER(Nn=50,MAXN=2*Nn,MAX2N=2*MAXN)
      COMPLEX X(MAXN,MAXN),T(MAXN,MAX2N),S,R,TM(MAXN,MAXN)
C        SUBROUTINE TO INVERT A MATRIX
C        USES THE GAUSS-JORDAN METHOD
      ISGN=1
      DO 1 I=1,N
      DO 1 J=1,N
      T(I,J)=X(I,J)
1     CONTINUE
      R=CMPLX(0.0,0.0)
      S=CMPLX(1.0,0.0)
      J1=N+1
      J2=N+N
      DO 2 I=1,N
      DO 2 J=J1,J2
    2 T(I,J)=R
```

```
      DO 3 I=1,N
      J=I+N
    3 T(I,J)=S
C         READY TO START PIVOTAL CONDENSATION ON ROW K
      DO 11 K=1,N
      KP=K+1
      IF(K.EQ.N)GO TO 6
C         FIND LARGEST ELEMENT IN COLUMN K
      L=K
      V=CABS(T(K,K))
      A=REAL(V)
      DO 4 I=KP,N
      V=CABS(T(I,K))
      B=REAL(V)
      IF(B.LE.A)GO TO 4
      L=I
      A=B
    4 CONTINUE
      IF(L.EQ.K)GO TO 6
C         INTERCHANGE ROWS L AND K
      ISGN=-ISGN
      DO 5 J=K,J2
      R=T(K,J)
      T(K,J)=T(L,J)
    5 T(L,J)=R
C         DIVIDE ROW K BY THE DIAGONAL
    6 R=T(K,K)
      TST=1.E-30
      IF(CABS(R).GE.TST) GO TO 60
      WRITE(LU,61)
61      FORMAT(1X,'MATRIX APPEARS SINGULAR - FOUND A ZERO
PIVOT')
        DO 50 I=0,N-1
        DO 50 J=0,N-1
        T(I,J)=CMPLX(0.,0.)
 50     CONTINUE
      RETURN
60    CONTINUE
      R=S/R
      DO 7 J=KP,J2
    7 T(K,J)=T(K,J)*R
C         ELIMINATE ELEMENTS IN COLUMN ABOVE K
      IF(K.EQ.1)GO TO 9
      KM=K-1
```

```
      DO 8 I=1,KM
      R=T(I,K)
      DO 8 J=KP,J2
    8 T(I,J)=T(I,J)-R*T(K,J)
C          ELIMINATE ELEMENTS IN COLUMN BELOW K
    9 IF(K.EQ.N) GO TO 12
      DO 10 I=KP,N
      R=T(I,K)
      DO 10 J=KP,J2
   10 T(I,J)=T(I,J)-R*T(K,J)
   11 CONTINUE
C          INVERSE IS COMPLETE
12    CONTINUE
      DO 14 I=1,N
   14 S=S*T(I,I)
      IF(ISGN.LT.0)S=-S
      DO 13 I=1,N
      DO 13 J=1,N
      K=J+N
      T(I,J)=T(I,K)
13    CONTINUE
        do 99 i=1,n
        do 99 j=1,n
        tm(i,j)=t(i,j)
 99     continue
      RETURN
      END

      subroutine  EPSL(FREQ,W,EEFFF,WEFFF,XIFFF)
        COMMON/CONST/PI,AMU0,EPS0,EPSEFF(6),OMEGA,WEFF(6),NUM
        COMMON/DIM/ A,B,C,D,D1,D2,H,ER,G,tt
      dimension p(40),r(50),eps(2),csl(2)
        EEFF0=EPS0
        EPSR=ER
      up = w/h
      th = tt/h
      f9 = freq/1.0e09
      F=F9*H
      if(th.lt.0.0000001e0) th = .0000001e0
      do 100 icount = 1,2
      eps(1) = 1.00001
      eps(2) = epsr
      e = eps(icount)
      call single(up,th,e,u)
```

```
      P(1) = 1.e0+ALOG((U**4+(U/52.e0)**2)/(U**4+.432e0))/49.e0
      P(1) = P(1)+ALOG(1.e0+(U/18.1e0)**3)/18.7e0
      P(2) = .564e0 * ((E-.9e0)/(E+3.e0))**.053e0
      E1   = (E+1.e0)/2.e0+(E-1.e0)*(1.e0+10.e0/U)**(-P(1)*P(2))/2.e0
      P(3) = .27488e0+(.6315e0+.525e0/(1.e0+.0157e0*F)**20)*U
      P(3) = P(3)-.065683e0*EXP(-8.7513e0*U)
      P(4) = .33622e0*(1.e0-EXP(-.03442e0*E))
      P(5) = .0363e0*EXP(-4.6e0*U)*(1.e0-EXP(-(F/38.7e0)**4.97e0))
      P(6) = 1.e0+2.751e0*(1.e0-EXP(-(E/15.916e0)**8))
      Q1   = P(3)*P(4)*((.1844e0+P(5)*P(6))*F)**1.5763e0
      E2   = E-(E-E1)/(1.e0+Q1)
      call single(up,th,e,u)
      ZO   = 376.77e0
      RO   = 6.e0+(2.e0*3.14159e0-6.e0)*EXP(-(30.666e0/U)**.7528e0)
      Z1   = ZO/2.e0/3.14159e0/SQRT(E1)*ALOG(RO/U+SQRT(1.e0+(2./U)**2))
      R(1) = .03891e0*E**1.4e0
      IF (R(1).le.20.e0) goto 10
      R(1) = 20.e0
   10 R(2) =.267e0*U**7
      IF (R(2).le.20.e0) goto 20
      R(2) = 20.e0
   20 R(3) = 4.766e0*EXP(-3.228e0*U**.641e0)
      R(4) =.016e0+(.0514e0*E)**4.524e0
      R(5) = (F/28.843)**12
      R(6) = 22.2e0*U**1.92e0
      IF (R(6).le.20.e0) goto 30
      R(6) = 20.e0
   30 R(7) = 1.206e0-.3144e0*EXP(-R(1))*(1.e0-EXP(-R(2)))
      R(8) = 1.+1.275*(1.-EXP(-.004625*R(3)*E**1.674e0*
     *       (F/18.365)**2.745))
      R(9)  = 5.086*R(4)*R(5)/(.386*R(4))*EXP(-R(6))/
     *       (1.+1.12992*R(5))
      R(9)  = R(9)*(E-1.)**6/(1.+10.*(E-1.)**6)
      R(10) = .00044*E**2.136+.0184
      R(11) = (F/19.47)**6/(1.+9.619999-2*(F/19.47)**6)
      R(12) = 1./(1.+.00245*U**2)
      R(13) = .9408*E2**R(8)-.9603
      R(14) = (.9408-R(9))*E1**R(8)-.9603
      R(15) = .707*R(10)*(F/12.3)**1.097
      R(16) = 1.0 + .05030*E**2*R(11)*(1.0-EXP(-(U/15.0)**6))
      R(17) = R(7)*(1.0-1.12410*R(12)/R(16)*EXP(-.0260*
     *       F**1.156560-R(15)))
      Z2    = Z1*(R(13)/R(14))**R(17)
      csl(icount) = sqrt(e1)/(3.e8*z1)
```

```
100   continue
      e11 = csl(2)/csl(1)
      z11 = sqrt(e11)/(3.e8*csl(2))
      e22 = e2*e11/e1
      z22 = z2*z11/z1
      eeff0 = e11
      eefff = e22
      zair  = 376.73
      weff0 = zair/z11*h/sqrt(e11)
      wefff = zair/z22*h/sqrt(e22)
      BB1=1.+UP**.371/(1.0+2.3580*EPSR)
      PP4=1.0+.03770*ATAN((.0670*UP**1.4560)*(6.0-5.0*EXP(
     *    .0360*(1.0-EPSR))))
      PP3=.52740*ATAN(.0840*UP**(1.94130/BB1))
      PP3=1.0+PP3/(E22**.92360)
      PP2=1.0-.2180*EXP(-7.50*UP)
      PP1=.4349070*(UP**.85440+.2360)*(E22**.810+.260)/
     *    ((UP**.85440+.870)*(E22**.810-.1890))
      XLEX=H*PP1*PP2*PP3/PP4
      DWE=(WEFFF-UP*H)/2.0
      XLFF=1.0-(2.0*DWE*UP*H+DWE*DWE-2.0*XLEX*UP*H-XLEX**2)/
     *    (WEFFF**2)
        end

      subroutine single(up,th,e,u)
      parameter (pi = 3.14159265358)
      dws = sqrt(6.517*up)
      dws = th*(log(1.0+10.87313/(th*((exp(2.0*dws)+1.0)/
     *      (exp(2.0*dws)-1.0))**2)))/pi
      dwr = .50*(1.0+2.0/(exp(sqrt(e-1.0))+exp(-
     *      (sqrt(e-1.0)))))*dws
      u = dwr + up
      end
```